28
5-9-78
25 to 27 TO

BNL-NUREG-23131

FRACTURE MECHANICS APPROACHES FOR ASSESSMENT OF HTGR STEAM GENERATOR TUBE WELD INTEGRITY

T. TANAKA*, P. BEZLER, AND M. SUBUDHI

* On leave from Japan Atomic Energy Research Institute.

Date Published - August, 1977

DEPARTMENT OF APPLIED SCIENCE BROOKHAVEN NATIONAL LABORATORY
UPTON, NEW YORK 11973

MASTER

Prepared for the U.S. Nuclear Regulatory Commission
Office of Nuclear Regulatory Research
Contract No. EY-76-C-02-0016

DISTRIBUTION OF THIS DOCUMENT IS UNLIMITED

BNL-NUREG-23131
INFORMAL REPORT

FRACTURE MECHANICS APPROACHES FOR ASSESSMENT OF HTGR STEAM GENERATOR TUBE WELD INTEGRITY

by

T. Tanaka*, P. Bezler, and M. Subudhi

Structures Analysis Group

Department of Applied Science
Brookhaven National Laboratory
Upton, NY 11973

NOTICE MN ONLY

PORTIONS OF THIS REPORT ARE ILLEGIBLE. It has been reproduced from the best available copy to permit the broadest possible availability.

July, 1977

NOTICE

This report was prepared as an account of work sponsored by the United States Government. Neither the United States nor the United States Department of Energy, nor any of their employees, nor any of their contractors, subcontractors, or their employees, makes any warranty, express or implied, or assumes any legal liability or responsibility for the accuracy, completeness or usefulness of any information, apparatus, product or process disclosed, or represents that its use would not infringe privately owned rights.

NOTICE: This document contains preliminary information and was prepared primarily for interim use. Since it may be subject to revision or correction and does not represent a final report, it should not be cited as reference without the expressed consent of the author(s).

* On leave from Japan Atomic Energy Research Institute.

DISTRIBUTION OF THIS DOCUMENT IS UNLIMITED

TABLE OF CONTENTS

	Page
Abstract	i
List of Tables and Figures	ii
1. Introduction	1
2. Weld Geometry	3
3. Material Data	4
4. Loading Conditions	4
5. Computer Program "APES"	5
6. Results of the Analyses	12
7. Conclusions	14
8. Acknowledgments	16
References	17
Appendix	42

Abstract

HTGR steam generator tube welds with circumferential cracks in their highest stress region were assessed by linear elastic fracture mechanics methods. The computed stress intensity factors were below the threshold level for propagation and crack propagation will not occur for the pipe geometry (radius and thickness of tube wall) and the stress levels considered. In addition crack arrest may be expected if the predominant stress field is a thermally induced bending stress field.

List of Tables and Figures

Table 1	Tube dimensions
Table 2	Material data
Table 3	Loading conditions
Table 4	Computed stress intensity factors [psi$\sqrt{in}$ units]

Figure 1a, b	HTGR steam generator tube weldment
Figure 2	QUAD-12 finite element and local element node numbers
Figure 3a, b	Special core element crack tip models
Figure 4	Tube crack free stress distributions superheater tube, I800/I82/I800 stress free at 70°F
Figure 5	Tube crack free stress distributions reheater tube, I800/I82/I800 stress free at 70°F
Figure 6a, b	Tube crack free stress distributions superheater tube, I800/I82/2 1/4 Cr-Mo stress free at 70°F
Figure 7a, b	Tube crack free stress distributions superheater tube, I800/I82/I800 stress free at 1350°F
Figure 8a, b	Tube crack free stress distributions reheater tube, I800/I82/I800 stress free at 1350°F
Figure 9a, b, c, and d	Tube crack free stress distributions superheater tube, I800/I82/2 1/4 Cr-Mo stress free at 1350°F

List of Tables and Figures (continued)

Figure 10 Tube crack free fine stress distributions

superheater tube, I800/I82/I800
stress free at 1350°F

Figure 11 Tube crack free fine stress distributions

reheater tube, I800/I82/I800
stress free at 1350°F

Figure 12a, b Tube crack free fine stress distributions

superheater tube, I800/I82/2 1/4 Cr-Mo
stress free at 1350°F

Figure 13 Idealizations for fracture mechanics calculations

Figure 14 Computed stress intensity factors at operating temperature, stress free at 1350°F

Figure 15 Computed stress intensity factors at room temperature, stress free at 1350°F

Figure A-1 Idealization of single-edge crack by enriched QUAD-12 elements

Figure A-2 Idealization of single-edge crack by core element with 13 nodes

Figure A-3 Idealization of 45-degree slant crack in tension specimen

Figure A-4 Idealization of single-edge crack by core element with 19 nodes

Figure A-5 Idealization of cracked bar

Figure A-6 Idealization of cylinder with internal circumferential crack

Figure A-7 Idealization of cylinder with internal axial crack

Figure A-8 Crack opening stress $\sigma(x)$ distribution

1. Introduction

The justification for applying fracture mechanics approaches to the evaluation of tube weldments derives from the hypothesis that cracks, flaws, and defects may exist in the steam generator tube welds. The approach is then directed toward supplying quantitative information on questions such as:

1. What are the critical crack sizes (i.e., sizes required to cause failure) in the various portions of steam generator tube welds at the expected test and/or operational stress levels?
2. Will cracks initially present, but below critical size, grow to critical size and cause failure during the expected service life of the steam generator?
3. If a critical crack size does exist, will the resulting failure be relatively small in extent, causing a major break in the steam generator?

It may be noted that these three questions involve the three aspects of fracture mechanics analyses:

1. Crack-growth initiation.
2. Crack propagation.
3. Crack propagation arrest.

Small flaws or cracks may grow when subjected to cyclic loads (fatigue), aggressive environments (corrosion fatigue and stress corrosion), or a combination of all these factors. A crack in a tube wall will propagate perpendicularly to the main stress axis. Thus, a crack will advance through the wall thickness at a rate faster than it elongates in the longitudinal or circumferential directions. Having extended through the wall, the crack produces either a leak or a rupture, depending on whether the crack has reached a critical length. A subcritical crack producing leakage may grow longitudinally causing a bulging failure.

To assess the integrity of the HTGR steam generator tube welds, linear elastic fracture mechanics methods were used to evaluate the characteristics of circumferential cracks in tubes with representative dimensions supporting operating loads. In these analyses, the materials were assumed to retain their virgin material mechanical properties. As a refinement of this procedure, the change in the mechanical properties of these materials due to the long-term exposure to elevated temperatures must be made.

Several analysis techniques may be used to solve problems of stress and strain singularities at crack tips. With the finite element method, the singularities may be characterized in the following ways.[1]

1. Direct Method - Conventional elements are used defining the region near the singularity with an extremely fine grid. This is obviously a very costly and inefficient procedure.

2. Energy Release Method - Conventional elements are used defining the singular region with a relatively fine grid. The energy of the system is then monitored as the crack length grows (i.e., several static solutions with increasing crack length are run). This method proves to be more accurate than that shown in Ref. (1) and requires significantly fewer elements, but it remains awkward and time consuming and requires the solution to several similar problems. One drawback of this method is the inability to distinguish between Mode I and Mode II intensities.

3. Superposition Method - Conventional elements with coarse grids are used in conjunction with a classical solution. The method is somewhat cumbersome.

4. Singularity Function Formulations - A special element is formulated that contains the proper singularity. This procedure requires the formulation

of a complicated element stiffness matrix but can be coupled easily to conventional elements. Coarse meshing gives very accurate results.

The present analyses were conducted with the APES[2] finite element computer program. This code uses a singularity function formulation to model elastic bodies with singular points. The latest version of APES contains subroutines that calculate the state of strain at the tip of a crack in either plane stress, plane-strain,or axisymmetric geometries. Linear isotropic stress-strain material properties are used and small strain theory is assumed.

2. Weld Geometry

The structural evaluations were performed using the standard weld joint geometry shown in Figure 1a. Various combinations of base metal and weld filler metal were considered. The material combinations and the tube dimensions treated are summarized in Table 1.

Table 1

	Tube Dimensions		
	Material	Inner Radius	Thickness
Superheater Tube	Incoloy 800 (Inconel 82)	0.3625"	0.2"
Superheater Tube	Incoloy 800 + 2 1/4 Cr-Mo (Inconel 82)	0.3625"	0.2"
Reheater Tube	Incoloy 800 (Inconel 82)	0.6725"	0.14"

3. Material Data

The material properties employed in the study for both base and filler metals are shown in Table 2.[3] No attempt was made to account for base metal dilution or its effect upon the properties.

Table 2

Material Data

	Temp.	Incoloy 800	Inconel 82	2 1/4 Cr.Mo
Modulus of Elasticity (psi)	900°F	23.9×10^6	27.85×10^6	26.05×10^6
	1030°F	23.4×10^6	27.1×10^6	---
Poisson's Ratio	900°F	0.365	0.3075	0.289
	1030°F	0.367	0.314	---
Thermal Coefficient of Expansion ($°F^{-1}$)	900°F	9.3×10^{-6}	8.25×10^{-6}	7.65×10^{-6}
	1030°F	9.4×10^{-6}	8.4×10^{-6}	---

4. Loading Conditions

The tubes were evaluated for the expected normal conditions of operation, both thermal and pressure. In addition, as regard to thermal stresses, the initial stress free state was chosen to correspond to both 1350°F and 70°F. The lower temperature corresponds to analyses wherein welding operation induced residual stress effects are ignored while the higher temperature allows some accounting of these effects.

Table 3

Loading Conditions

	He Side Pressure	Steam Side Pressure	Tube Temp.	Radial Gradient
Superheater Tube	710 psi	2,600 psi	900°F	50°F
Superheater Tube (Bimetallic)	710 psi	2,600 psi	860°F	45°F
Reheater Tube	725 psi	640 psi	955°F	85°F

5. Computer Program "APES" (2)

APES is an acronym for "Axisymmetric/Planar Elastic Structures". It is a finite element computer program which incorporates a 12-node quadrilateral isoarametric element having a bicubic displacement assumption and adapted to plane strain, plane stress and axisymmetric conditions of structural behavior. For linear elastic fracture mechanics applications, two different special elements are employed for predicting stress intensity factors: (1) a small circular "core" element which surrounds the crack tip and which reproduces the singular nature of the stresses there, and (2) "enriched" 12-node isoparametric elements which have the elastic singular solution superimposed so that a corner node corresponds to a crack tip. The formulations of these elements are outlined briefly here to indicate the finite element approximations involved in the use of the APES computer program.

1. Conventional Quad-12 Element

The Quad-12 element and its local, nonorthogonal (in general) coordinate system (s,t) are shown in Figure 2. The edges of the element correspond to values of s or t of $\pm$ 1, and the midside nodes correspond to values of s or t of $\pm$ 1/3.

The displacement assumptions for the QUAD-12 element are given by

$$U = \sum_{i=1}^{12} N_i (s,t)\, U_i$$

$$V = \sum_{i=1}^{12} N_i (s,t)\, V_i \qquad (1)$$

where U and V = x and y components of displacement U_i and V_i = the displacement components at node i.

N_i (s,t) = polynomials which interpolate the displacement over the element.

The element is made to be isoparametric (same parameters) by letting the geometry vary in a fashion as the displacements

$$x = \sum_{i=1}^{12} Ni (s,t)\, x_i$$

$$y = \sum_{i=1}^{12} N_i (s,t)\, y_i \qquad (2)$$

where x and y define positions within the element and x_i and y_i are the coordinates of Node i.

The specific N_i for the QUAD-12 element are given by

$$N_i = \frac{1}{32} (1-t)\,(1-s)\,[-10 + 9\,(s^2 + t^2)]$$

$$N_2 = \frac{9}{32} (1-t)\,(1-s^2)\,(1-3s)$$

$$N_3 = \frac{9}{32} (1-t)\,(1-s^2)\,(1+3s)$$

$$N_4 = \frac{1}{32} (1-t)\,(1+s)\,[-10 + 9\,(s^2 + t^2)]$$

$$N_5 = \frac{9}{32}(1+s)(1-t^2)(1-3t)$$

$$N_6 = \frac{9}{32}(1+s)(1-t^2)(1+3t)$$

$$N_7 = \frac{1}{32}(1+s)(1+t)[-10 + 9(s^2+t^2)]$$

$$N_8 = \frac{9}{32}(1+t)(1-s^2)(1+3s)$$

$$N_9 = \frac{9}{32}(1+t)(1-s^2)(1-3s)$$

$$N_{10} = \frac{1}{32}(1+t)(1-s)[-10 + 9(s^2+t^2)]$$

$$N_{11} = \frac{9}{32}(1-s)(1-t^2)(1+3t)$$

$$N_{12} = \frac{9}{32}(1-s)(1-t^2)(1-3t) \qquad (3)$$

It may be seen that the displacements within the element vary cubically as opposed to a linear variation in the constant-stress element. These shape functions are equivalent to a displacement assumption for a "conventional" quadrilateral finite element with sides parallel to the x- and y- axes given by

$$U = \alpha_1 + \alpha_2 x + \alpha_3 y + \alpha_4 x^2 + \alpha_5 xt + \alpha_6 y^2 + \alpha_7 x^3 + \alpha_8 x^2 y + \alpha_9 xy^2 + \alpha_{10} y^3 + \alpha_{11} x^3 y + \alpha_{12} xy^3$$

$$V = \alpha_{13} + \alpha_{14} x + \alpha_{15} y + \alpha_{16} x^2 + \alpha_{17} xy + \alpha_{18} y^2 + \alpha_{19} x^3 + \alpha_{20} x^2 y + \alpha_{21} xy^2 + \alpha_{22} y^3 + \alpha_{23} x^3 y + \alpha_{24} xy^3 \qquad (4)$$

where the α's are undetermined parameters (generalized coordinates). The

first three terms in each of Equations (4) correspond to the constant-stress triangular element; the remaining terms demonstrate the "higher order" of the QUAD-12 element. Note that the displacements vary cubically over the element and that the geometry of the element edges may also vary cubically in space, so that strains and stresses vary quadratically over the element.

2. "Core" Crack Tip Element

The special circular crack tip or "core element" is shown in Figure 3. The element is a half-disk for symmetric Mode I problems, and becomes a full circle for combined mode problems. The edges of the QUAD-12 elements that join the core element are curved, providing geometric continuity between the two element types.

The displacement assumption taken from the singular core element corresponds to the first (singular) terms of the elasticity series expansion for the displacements in the immediate vicinity of a crack tip. It has the form:

$$\begin{Bmatrix} U \\ V \end{Bmatrix} = \begin{Bmatrix} U_o \\ V_o \end{Bmatrix} + \frac{K_I}{4_G}\sqrt{\frac{r}{2\pi}} \begin{Bmatrix} \cos\alpha & -\sin\alpha \\ \sin\alpha & \cos\alpha \end{Bmatrix} \begin{bmatrix} (2K-1)\cos\frac{\sigma}{2} & -\cos\frac{3\sigma}{2} \\ (2K+1)\sin\frac{\sigma}{2} & -\sin\frac{3\sigma}{2} \end{bmatrix}$$

$$+ \frac{K_{II}}{4_G}\sqrt{\frac{r}{2\pi}} \begin{Bmatrix} \cos\alpha & -\sin\alpha \\ \sin\alpha & \cos\alpha \end{Bmatrix} \begin{bmatrix} (2K+3)\sin\frac{\sigma}{2} & +\sin\frac{3\sigma}{2} \\ (2K-3)\cos\frac{\sigma}{2} & -\cos\frac{3\sigma}{2} \end{bmatrix} \qquad (5)$$

where

K_I, K_{II} = Mode I and Mode II stress intensity factors

U, V = displacements

G = elastic shear modulus

K = (3-4ν) for plane strain or axisymmetric

(3-ν/1+ν) for plane stress

ν = Poisson's ratio

γ,σ = polar coordinates centered at the crack tip as shown in Figure 2. The corresponding stress field is $\sigma_{ij} = \sigma_{ij}(\gamma^{-1/2},\sigma)$ which tends to infinity as γ tends to zero.

The unknowns associated with the core element are the two crack tip displacements U_o and V_o and the stress intensity factors K_I and K_{II}. The singular core element is joined to the conventional QUAD-12 elements by requiring that the displacements of nodes that join the core element match the singular solution evaluated at γ_o (the outer radius of the core element) and at the appropriate angle σ. The fracture mechanics stress intensity factors are calculated at the same time as the nodal displacement. The incompatibility between the core and the standard finite elements has been found to be of negligible effect provided (1) a sufficient number of elements surround the core element (10 nodes have proven adequate for the Mode I half-disk element, implying that 19 nodes are adequate for the combined mode problem); and (2) that the radius of the core element γ_o is taken as 2 or 3 percent of the crack length, with a ratio of k (the basic dimension of the QUAD-12 element) to γ_o in the range of about 6 to 10. Note that thermal loading is not programmed for this element at the present time.

3. "Enriched" QUAD-12 Element

The effects of the singularity are included in this element by "enriching" a bicubic element displacement assumption with terms that give the proper singularity at node (s,t),

$$U(s,t) = \alpha_1 + \alpha_2 s + \alpha_3 t + \alpha_4 s^2 + \alpha_5 st + \alpha_6 t^2 + \alpha_7 s^3 + \alpha_8 s^2 t + \alpha_9 st^2 + \alpha_{10} t^3 + \alpha_{11} st^3 + \alpha_{12} ts^3 + K_I f_1(s,t) + K_{II} g_1(s,t) \quad (6)$$

where the α's are undetermined constants (as are K_I and K_{II}) and $f_1(s,t)$ and $g_1(s,t)$ are the second and third terms of the first of Equation (5) evaluated in terms of the local element coordinates s and t. A similar expression exists for the V component of displacement. In matrix form, Equation (6) may be written

$$U(s,t) = [P(s,t)]\ \{\alpha\} + K_I\ f_1(s,t) + K_{II}\ g_1(s,t)\ . \tag{7}$$

Evaluating Equation (7) at each of the nodes, the following matrix equation may be written

$$\{U\} = [C]\ \{\alpha\} + K_I\ \{f_1\} + K_{II}\ \{g_1\} \tag{8}$$

in which all matrices are known except $\{U\}$ and $\{\alpha\}$.

Solving Equation (8) for the unknown coefficients $\{\alpha\}$ in terms of the nodal displacements, U_i where i = 1, 12, the displacement assumption may be written as

$$U(s,t) = \Sigma\ N_i\ \bar{U}_i + K_I\ [f_1(s,t) - \Sigma\ N_i\ f_{1i}] + K_{II}\ [g_1(s,t) - \Sigma\ N_i\ g_{1i}] \tag{9}$$

where the subscripts on f_1 and g_1 indicate "evaluated at Node i". The analogous expression for the V-component of displacement is

$$V(s,t) = \Sigma\ N_i\ \bar{V}_i + K_I\ [f_2(s,t) - \Sigma\ N_i\ f_{2i}] + K_{II}\ [g_2(s,t) - \Sigma\ N_i\ g_{2}i]\ . \tag{10}$$

The terms enclosed in the parentheses in Equation (9) and (10) account for the singularity. An enriched QUAD-12 element connected to a standard QUAD-12 element would produce a slight incompatibility between the adjoining elements. This incompatibility can be removed by altering the displacement assumption of Equation (9) and (10) to

$$\begin{Bmatrix} U(s,t) \\ V(s,t) \end{Bmatrix} = \begin{Bmatrix} \Sigma\, N_i \bar{U}_i \\ \Sigma\, N_i \bar{V}_i \end{Bmatrix} + R(s,t) \begin{Bmatrix} K_I\,[f_1(s,t) - \Sigma\, N_i f_{1i}] + K_{II}[g_1(s,t) - \Sigma\, N_i g_{1i}] \\ K_I\,[f_2(s,t) - \Sigma\, N_i f_{2i}] + K_{II}[g_2(s,t) - \Sigma\, N_i g_{2i}] \end{Bmatrix} \quad (11)$$

where R(s,t) is chosen such that it equals 1 on boundaries adjacent to "enriched" elements and equals 0 on boundaries adjacent to standard elements.

Using the assumption given by Equation (11) in a standard finite element formulation, the left-hand side of the equilibrium equations for an element become

$$\begin{bmatrix} k^{11} & k^{12} \\ k^{21} & 0 \end{bmatrix} \begin{Bmatrix} \bar{U} \\ K_I \\ K_{II} \end{Bmatrix}$$

where

$\bar{U}$ = element nodal point displacements

k^{11} = "regular" stiffness matrix

k^{12} = coupled stiffness matrix from regular and enrichment terms

k^{21} = transpose (k^{12}).

Integration of k^{12} must be done very accurately because they contain singular terms. For this work a high order (8x8) gaussian quadrature is required for the enriched QUAD-12 elements.

6. Results of the Analyses

The stress analyses were conducted in two phases:

1. elastic calculations to determine the stress profiles in defect free tubes under normal conditions of loading;
2. fracture mechanics calculations to evaluate the effects of cracks in the most highly stressed regions.

The elastic analyses were performed with the APES code using only the conventional finite elements. For similar base metal weldments, symmetry about the weld center line was taken advantage of and the finite element grid (Figure 1b) had 514 nodes and 90 elements. For the general weldment, the grid was symmetric about the weld center line and contained 1,009 nodes and 180 elements. For each of the analyses nodes 496-514 were constrained in the longitudinal direction. Pressure loads were applied as radial forces to the inner and outermost nodes and, in addition, thermal loads were applied to each node with node-wise temperature distribution.

The pertinent results of the elastic analyses are depicted graphically in Figures 4-9. Figures 4, 5 and 6 correspond to the 70°F stress-free temperature state assumption while Figures 7, 8 and 9 to the 1350°F stress free state assumption. The results shown are traces of the radial, (σ_r), longitudinal (σ_z) and hoop (σ_θ) stresses along the inner and outer tube surfaces, node lines 1-496 and 19-514, respectively. Figures 4 and 7 correspond to the I800/I82/I800 superheater weldment, Figures 5 and 8 to the I800/I82/I800 reheater weldment, and Figures 6 and 9 to the I800/I82/2 1/4Cr-Mo weldment. For the cases corresponding to the 1350°F assumption, Figures 7-9, the stress states at room temperature and operating temperature are shown. In addition, in Figures 10, 11 and 12 the through thickness stress variations are shown for various node lines and each of the cases.

Referring to Figures 4-9 it is evident that for all cases strong stress gradients exist near the fusion zone, large through thickness (bending) variations exist, and the longitudinal stresses are greatest on the inner surface. For most cases the longitudinal stress component attains the peak stress levels. Referring to Figures 10-12 it is evident that strong through thickness bending stress gradients exist for the longitudinal and hoop stress components. Lastly, for all cases the longitudinal stress component attains its peak value on the inner surface near the fusion line.

For the fracture mechanics analyses, only circumferential cracks were considered. These result from either stress corrosion cracking or sustained load cracking and are commonly observed in tubes. For such cracks the longitudinal load or stress field is the dominant load parameter affecting both crack severity and growth characteristics. For a given weldment the most detrimental circumferential crack will be located at the point where the longitudinal stress component attains a maximum. From the elastic analyses this point is the fusion line at the inner surface for all the cases. This was taken as the crack location for all the fracture analyses.

For the fracture runs, enriched element crack tip models were employed. The gross finite element grid was similar to that used in the elastic analyses with adjustments in the vicinity of the crack. Figure 13 depicts exploded views of the grid surrounding the crack for crack lengths of 12.5, 25, 50, 75, and 87.5 percent of the wall thickness. Each weldment was analyzed for the 12.5% crack while the I800/I82/I800 superheater weldment was analyzed for all the crack lengths.

The computed stress intensity factors are summarized in Table 4 and shown graphically in Figures 14 and 15. Figure 14 shows the results

corresponding to the operating temperature stress fields while Figure 15 shows the results for the room temperature stress fields. In both cases the results are for the 1350°F stress free state assumption.

The computed stress intensity factors range from 1 to 4 Ksi$\sqrt{in}$. The highest computed factor is still below K_{th} (6 Ksi$\sqrt{in}$ @ 1000°F) for the material and consequently, there is no possibility of crack growth.[4] For the deep cracks, the presence of the crack itself markedly reduces the through wall thickness stress gradients and peak stresses which results in low values the stress intensity factors. This implies that if a small crack propagates in a tube wall having a steep stress gradient, crack arrest will occur after some propagation.

Table 4

Computed Stress Intensity Factors [psi$\sqrt{in}$ Units]

	$\frac{a}{b}$	Superheater Tube I800/I82/I800	Superheater Tube I800/I82/2 1/4Cr-Mo	Reheater Tube I800/I82/I800
	0.125	3834.4	3046.0	4040.2
Operating	0.125	3172.1 (temp. alone)		3931.8 (temp. alone)
Temperature	0.125	662.3 (press. alone)		
Stress Free at 1350°F	0.25	3799.6		
	0.50	2589.2		
	0.75	2460.8		
	0.875	3918.2		
	0.125	2690.0	966.3	1781.5
	0.25	1149.3		
Room	0.50	-1027.9		
Temperature	0.75	- 594.6		
Stress Free at 1350°F	0.875	1519.0		

7. Conclusions

An assessment of HTGR steam generator tube weld integrity has been completed. Circumferential cracks were evaluated using linear elastic fracture mechanics

theory. It was concluded that:

(a) Circumferential cracks do not propagate for the present pipe geometry (radius and thickness of tube wall) and the stress level.

(b) For thermally induced stress gradients, crack arrest may be expected if initial crack propagation does occur.

Acknowledgments

The authors wish to thank L. N. Gifford, Jr. for recommending the use of the APES computer code.

References

1. Benzley, S. E. and Beisinger, Z. E., "CHILES - A finite element computer program that calculates the intensities of linear elastic singularities," Sandia Laboratories Report SLA-73-0894 (September 1973).

2. Gifford, L. N., Jr., "APES - Second generation two-dimensional fracture mechanics and stress analysis by finite elements," NSRDC Report 4700 (December 1975).

3. Soo, P., "Analytical data for bimetallic weld structural evaluation," BNL Memorandum (February 1977).

4. Tanaka, Toshiyuki, "MODCRAK- Crack growth analysis computer program," BNL Report (to be published).

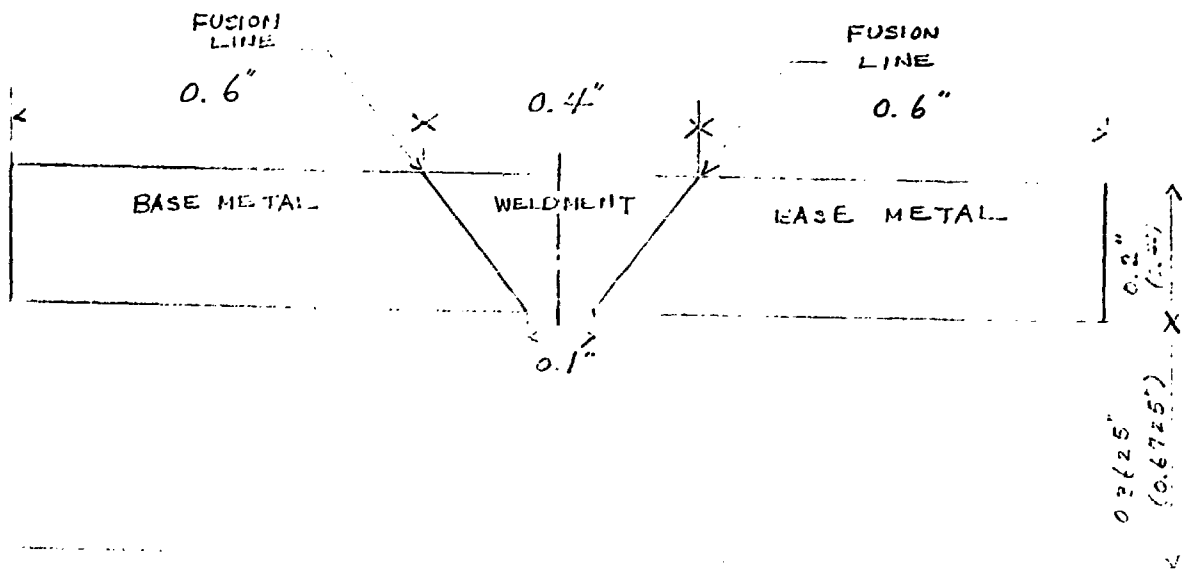

Figure 1 a . HTGR [illegible] Weldment

GRAPH PAPER GRAPHIC CONTROLS CORPORATION Buffalo, New York Printed in U.S.A. SQUARE 10 X 10 TO THE HALF INCH AS 0813 01

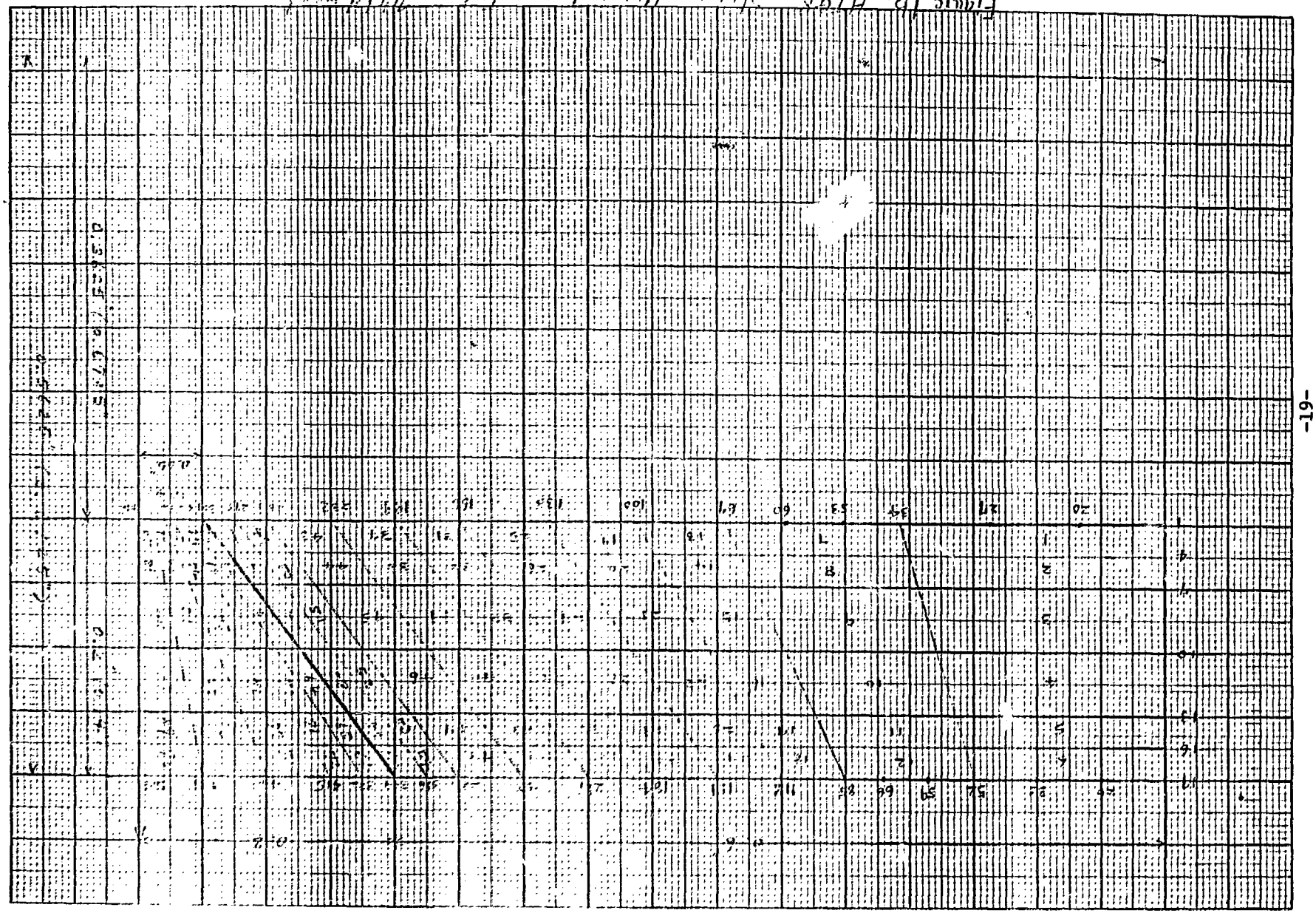

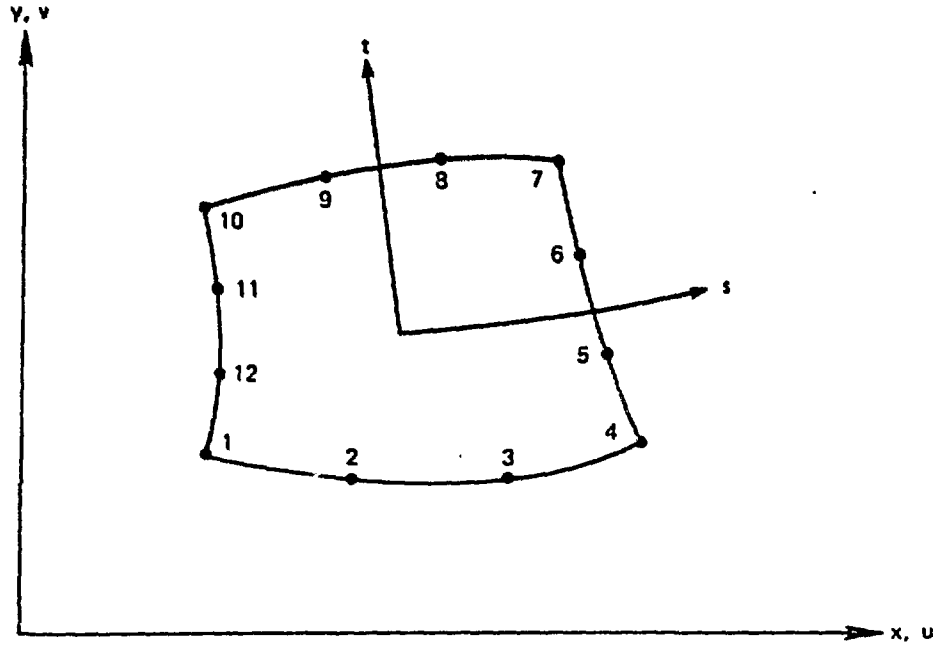

Figure 2 -- QUAD-12 Finite Element and Local Element Node Numbers

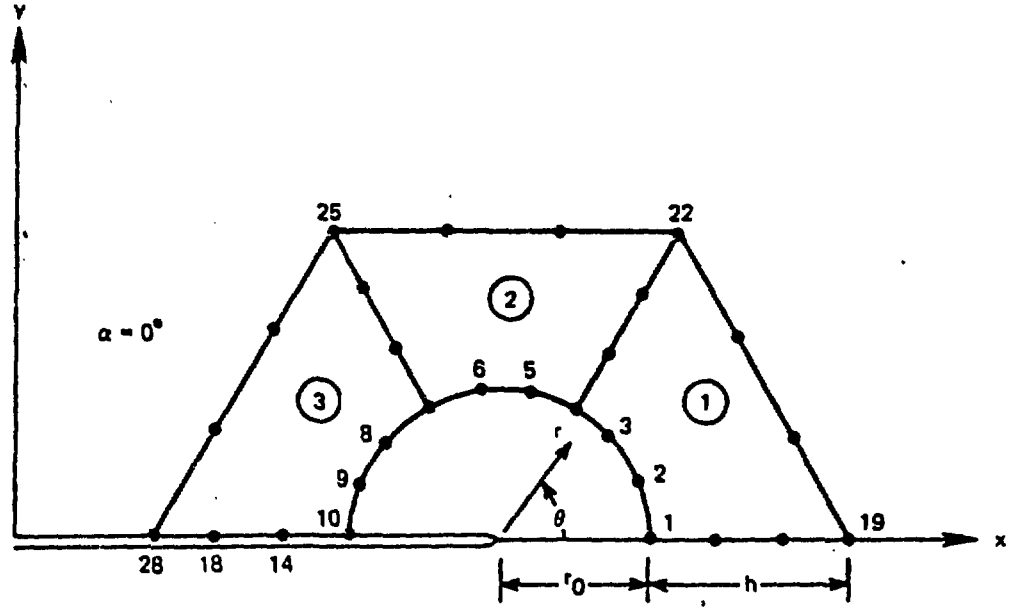

Figure 3a -- Mode I (Symmetric) Crack Tip Model

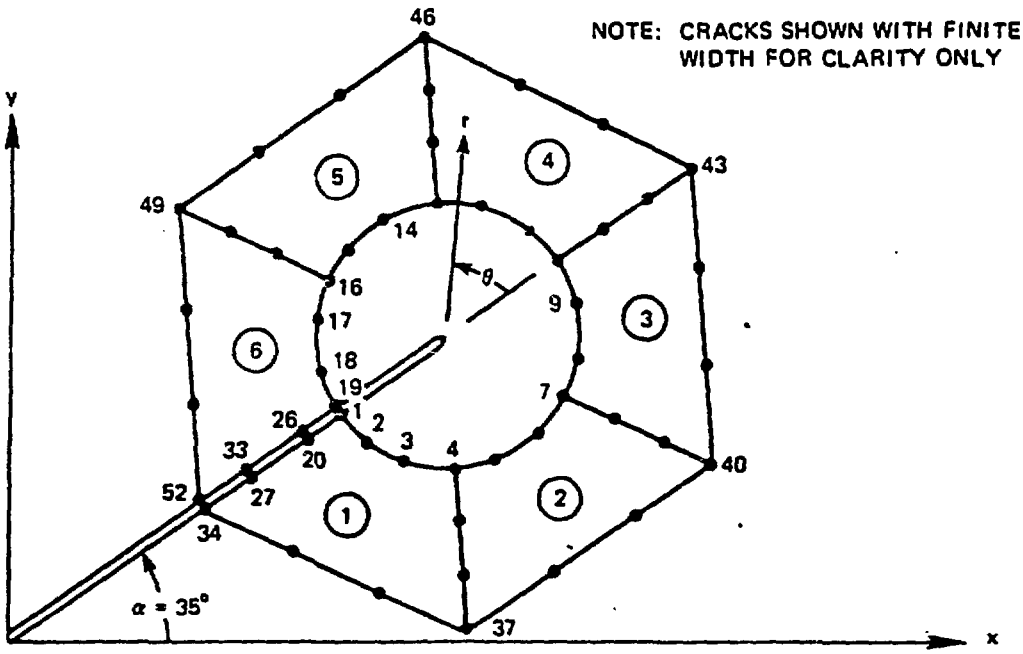

Figure 3b -- Combined Mode (Unsymmetric) Crack Tip Model

Figure 3 -- Special Core Element Crack Tip Models

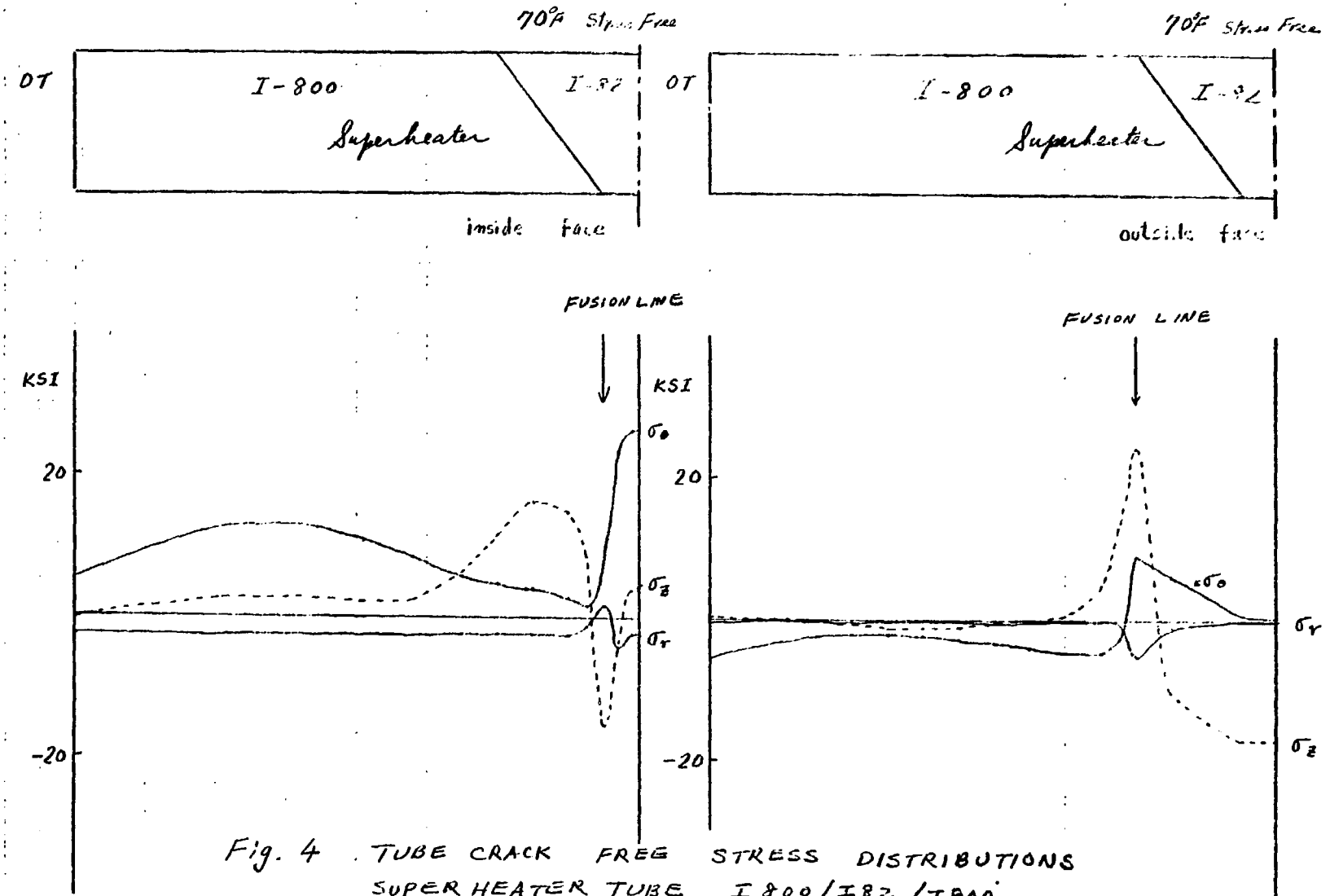

Fig. 4 TUBE CRACK FREE STRESS DISTRIBUTIONS
SUPER HEATER TUBE, I 800/I 82/I 800
STRESS FREE AT 70°F

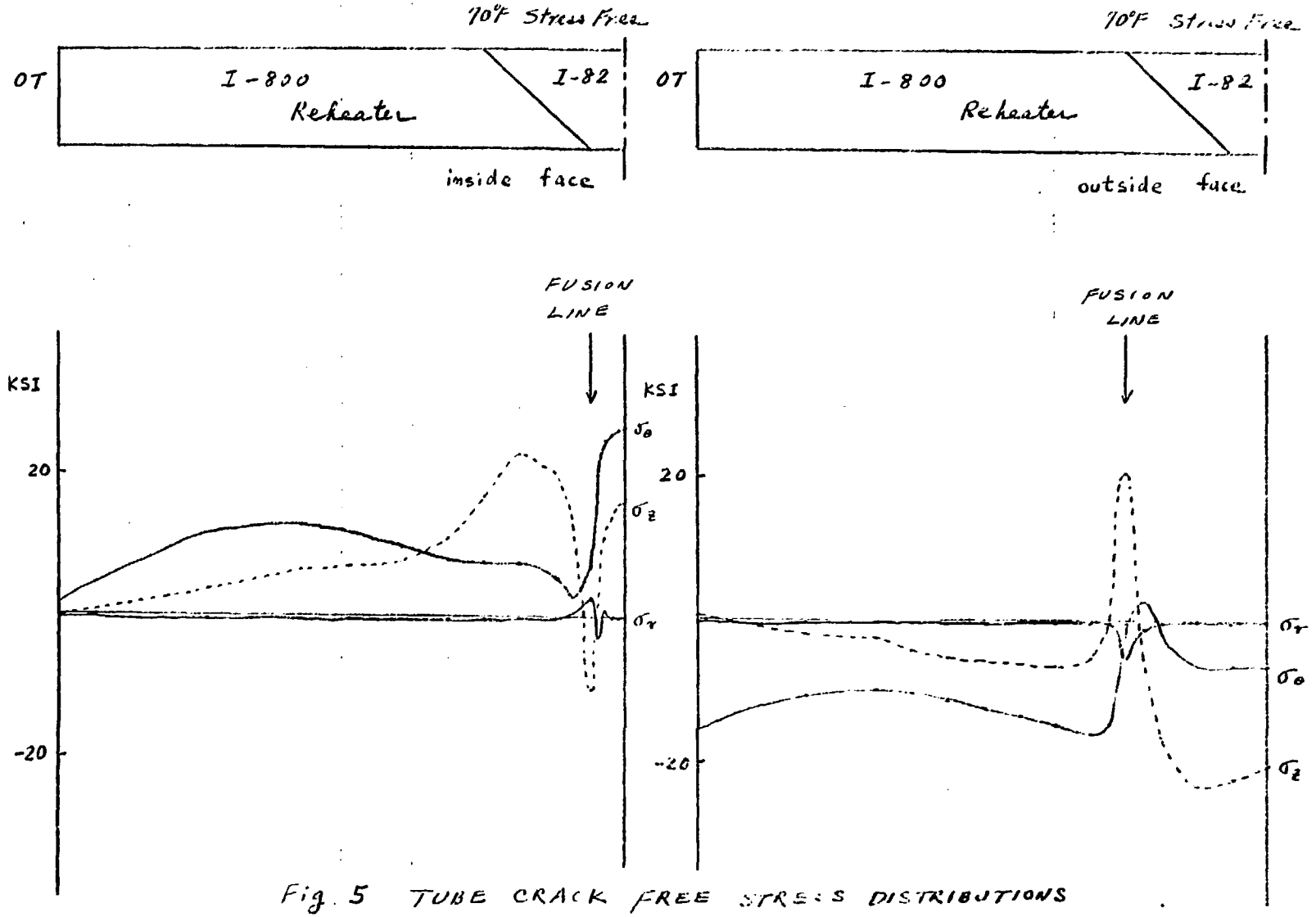

Fig. 5 TUBE CRACK FREE STRESS DISTRIBUTIONS
REHEATER TUBE, I 800/I 82/I 800
STRESS FREE AT 70°F

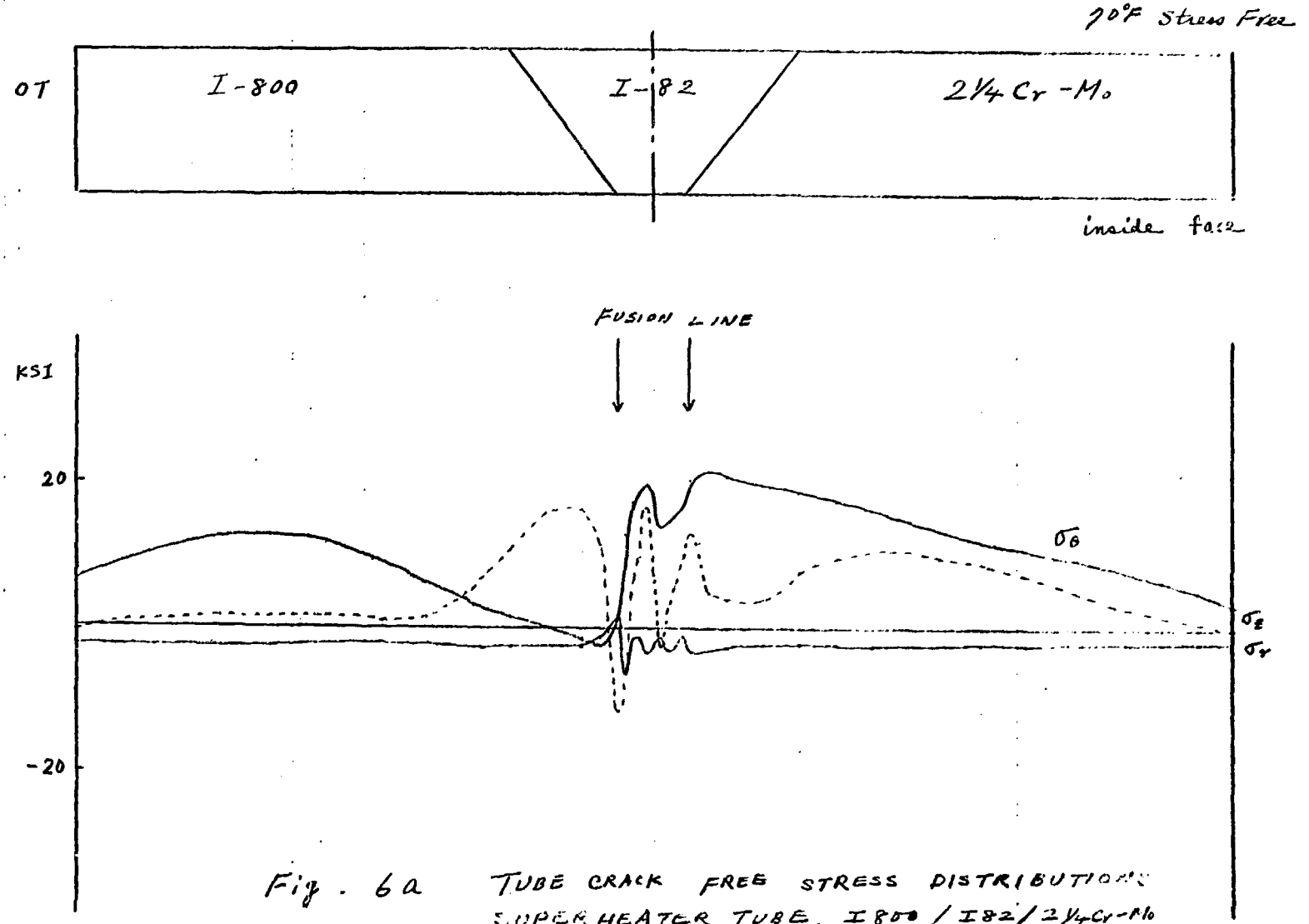

Fig. 6a TUBE CRACK FREE STRESS DISTRIBUTIONS SUPERHEATER TUBE, I800 / I82 / 2¼Cr-Mo STRESS FREE AT 70°F

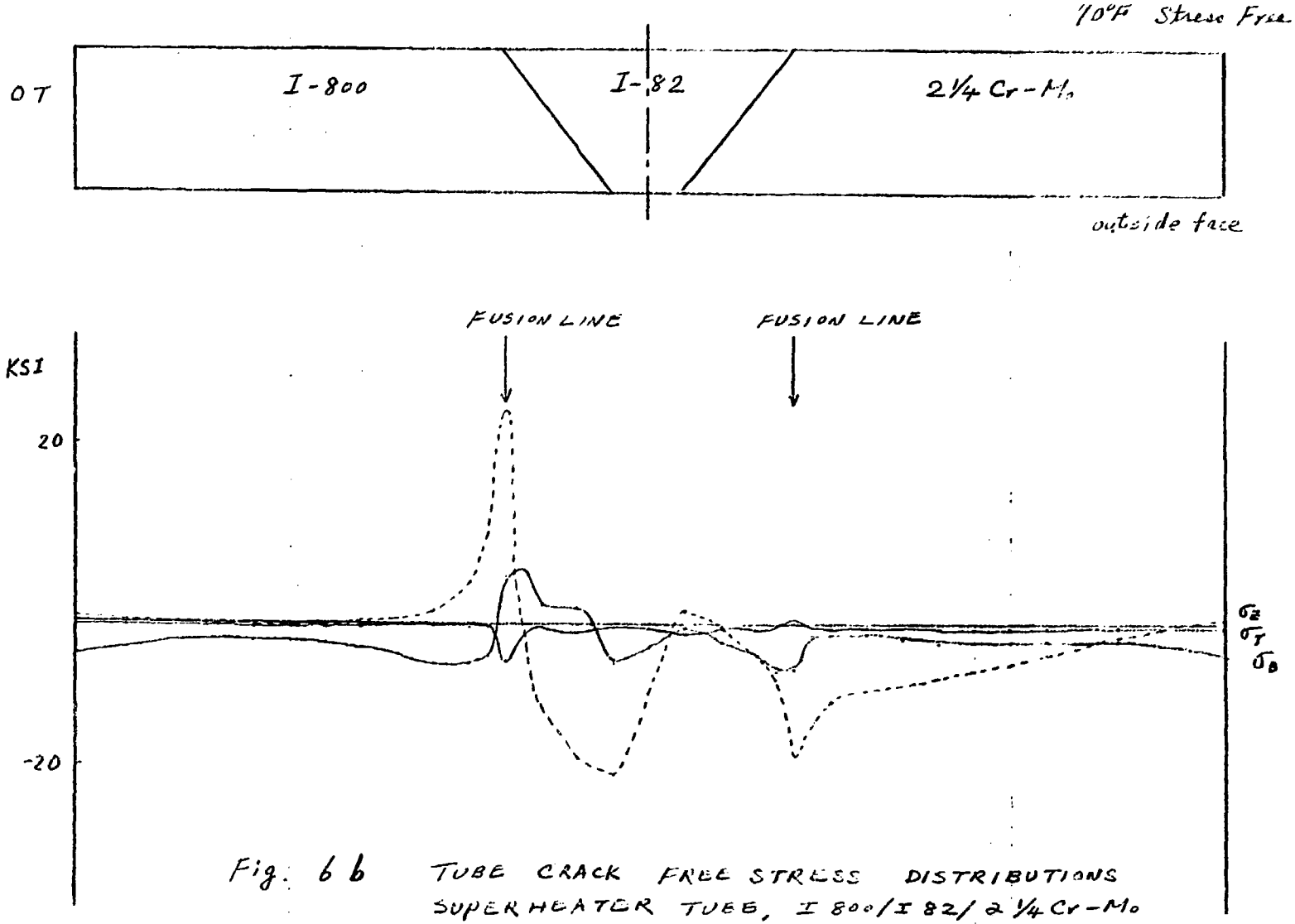

Fig. 6b TUBE CRACK FREE STRESS DISTRIBUTIONS SUPERHEATER TUBE, I 800/I 82/ 2¼ Cr-Mo STRESS FREE AT 70°F

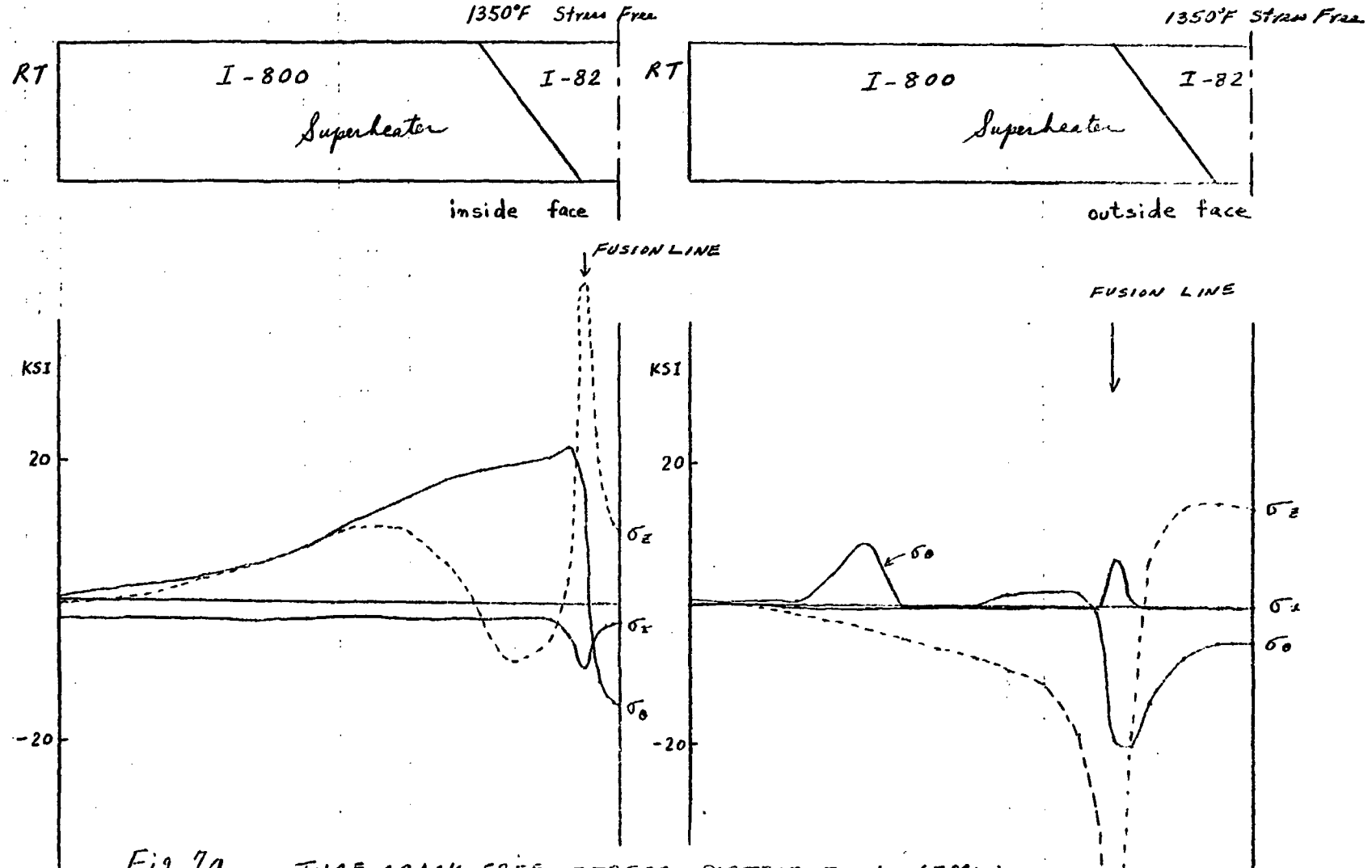

Fig. 7a TUBE CRACK FREE STRESS DISTRIBUTIONS (70°F)
SUPERHEATER TUBE, I800 / I82 / I800
STRESS FREE AT 1350°F

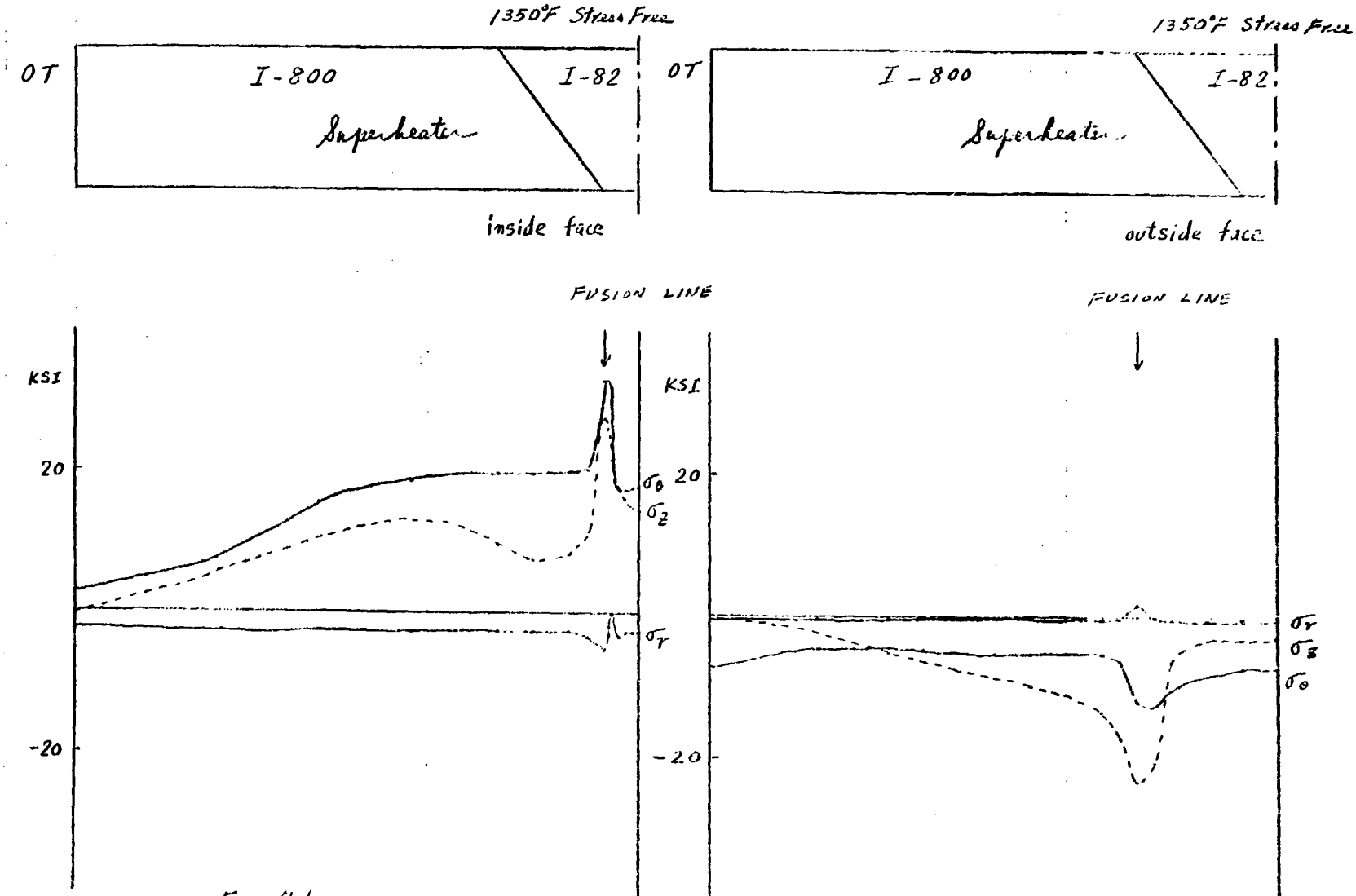

Fig. 16 TUBE CRACK FREE STRESS DISTRIBUTIONS
SUPERHEATER TUBE, I800/I82/I800
STRESS FREE AT 1350°F

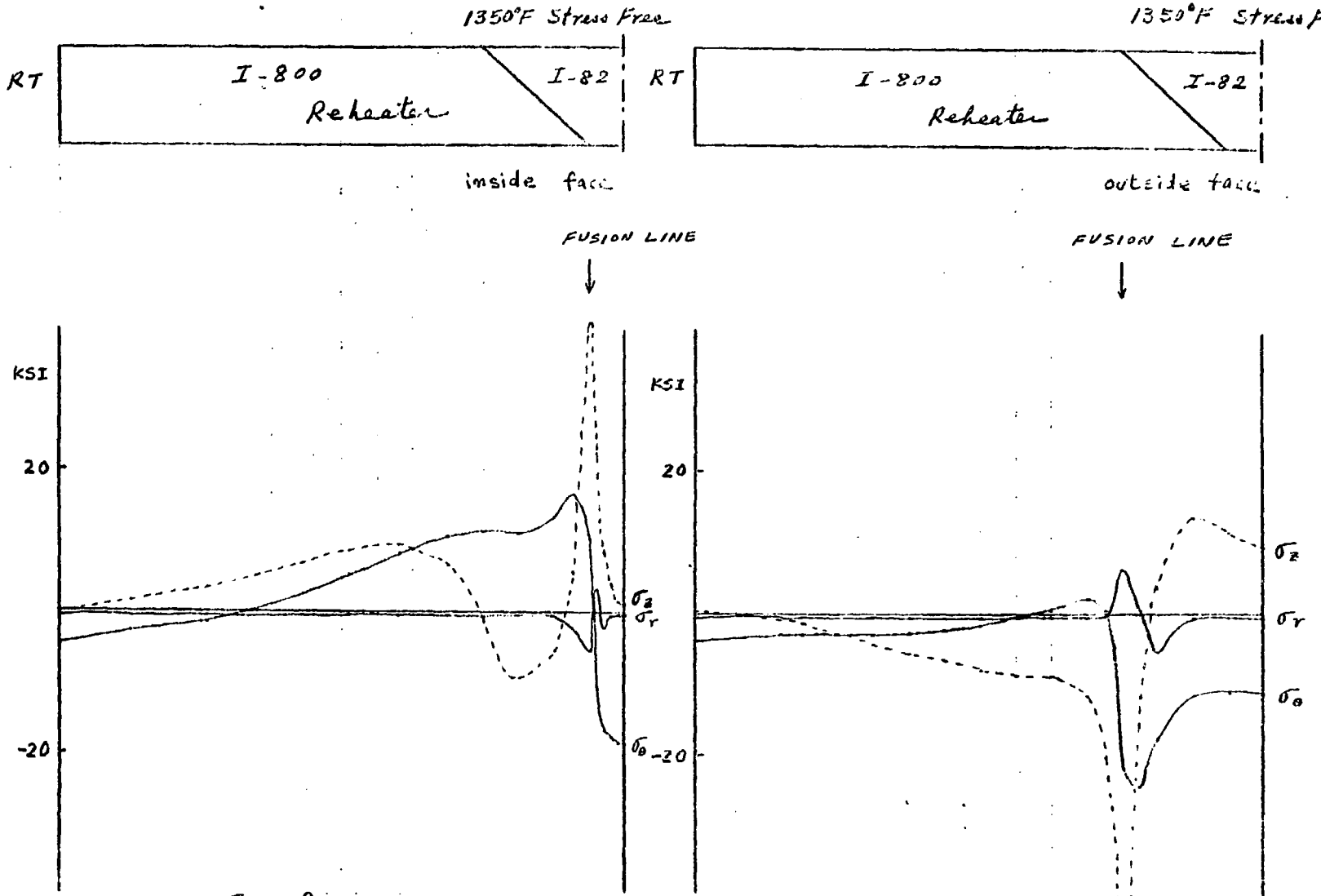

Fig. 8a TUBE CRACK FREE STRESS DISTRIBUTIONS (70°F)
REHEATER TUBE, I800/I82/I800
STRESS FREE AT 1350°F

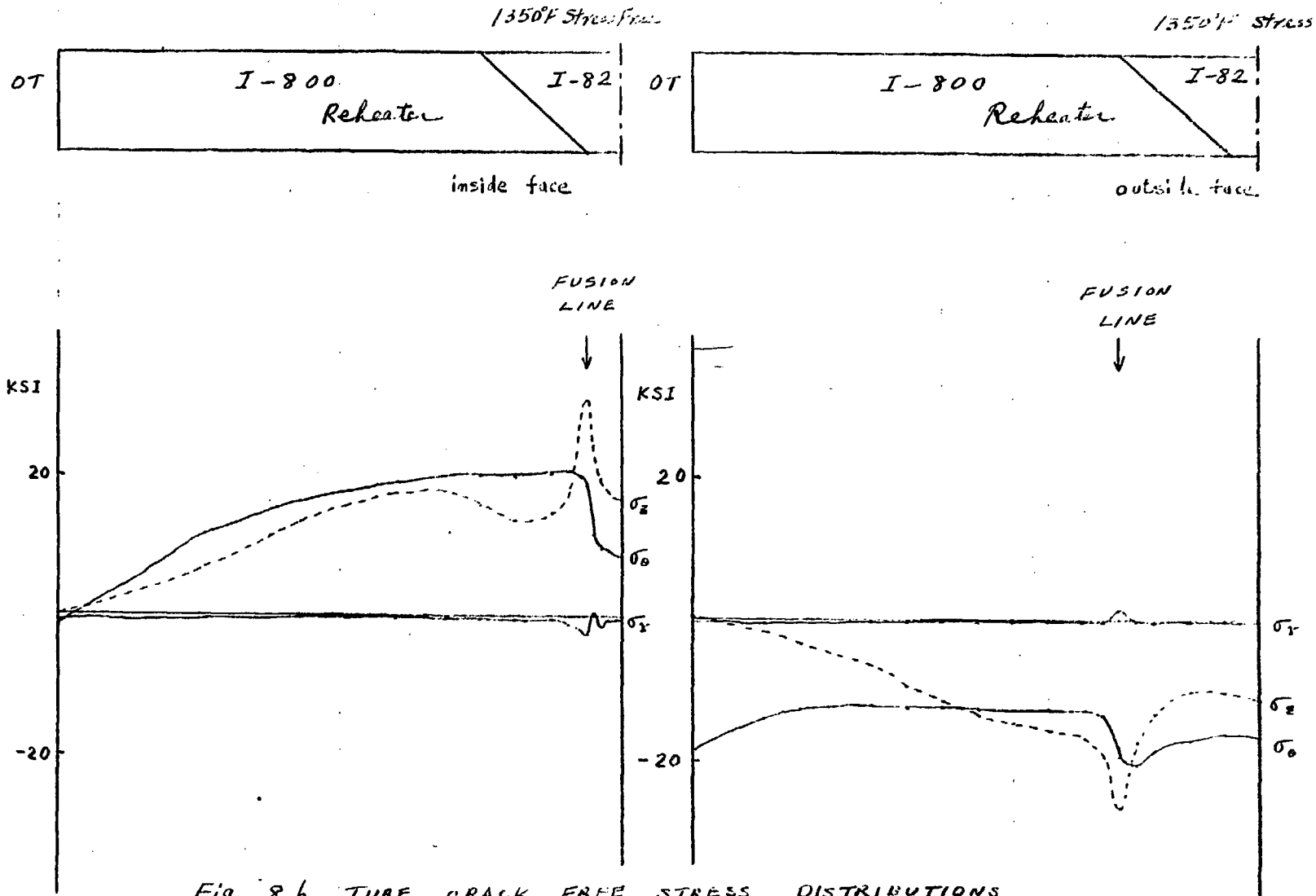

Fig. 8b TUBE CRACK FREE STRESS DISTRIBUTIONS
REHEATER TUBE, I800/I82/I800
STRESS FREE AT 1350°F

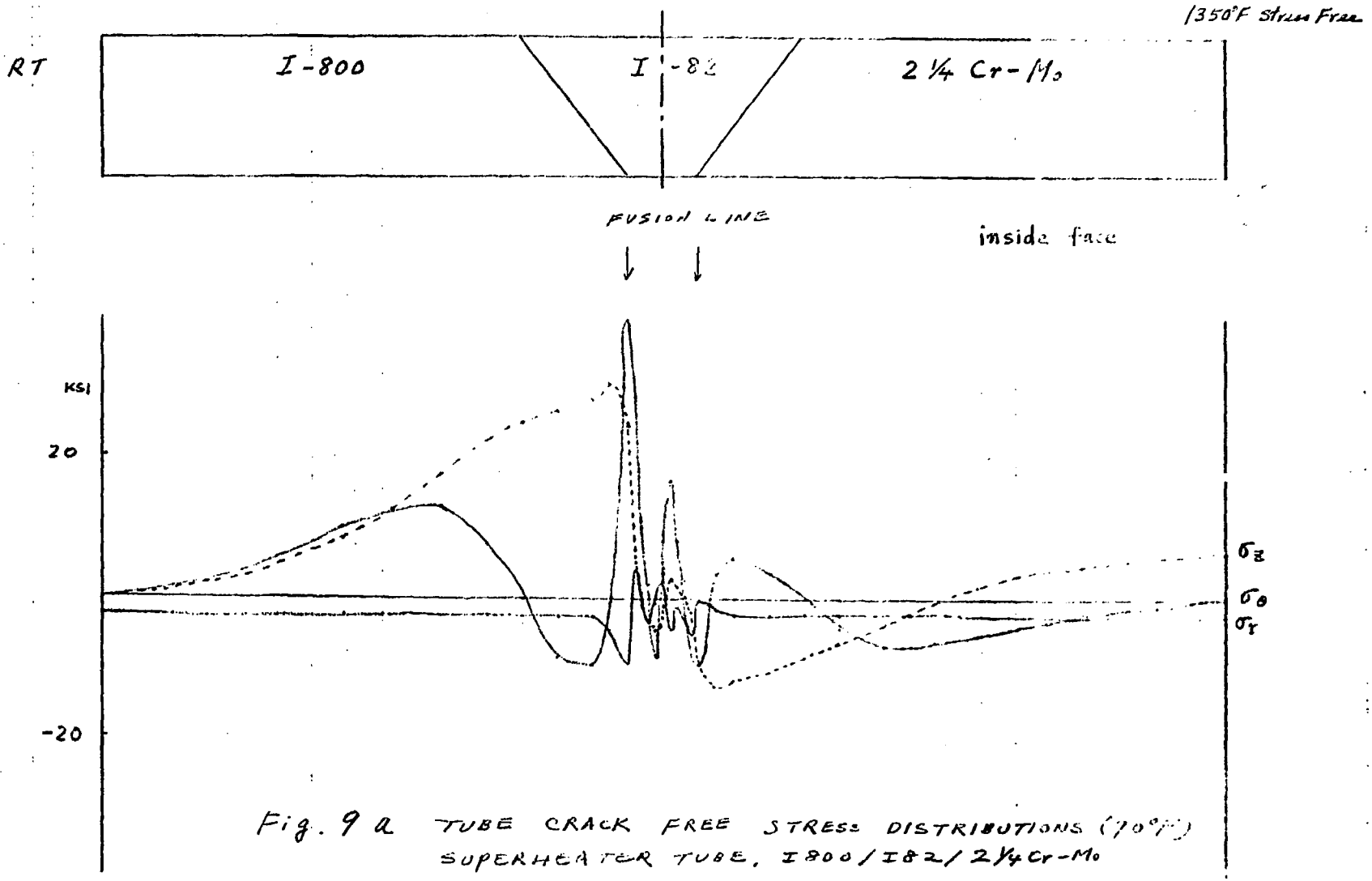

Fig. 9 a TUBE CRACK FREE STRESS DISTRIBUTIONS (70°F)
SUPERHEATER TUBE, I800/I82/2¼Cr-Mo
STRESS FREE AT 1350°F

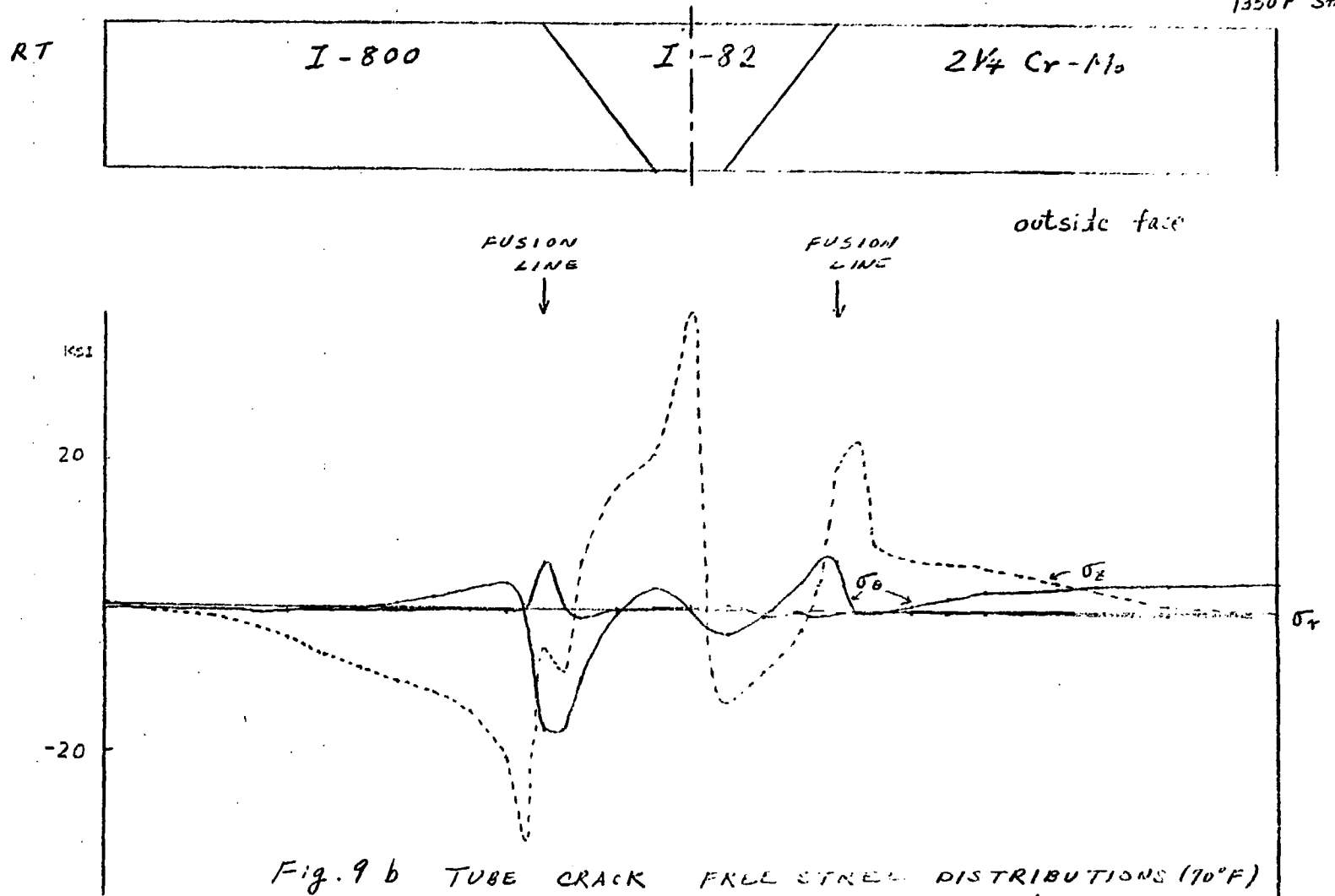

Fig. 9 b TUBE CRACK FREE STRESS DISTRIBUTIONS (70°F)
SUPERHEATER TUBE, I 800 / I 82 / 2¼ Cr-1Mo
STRESS FREE AT 1350°F

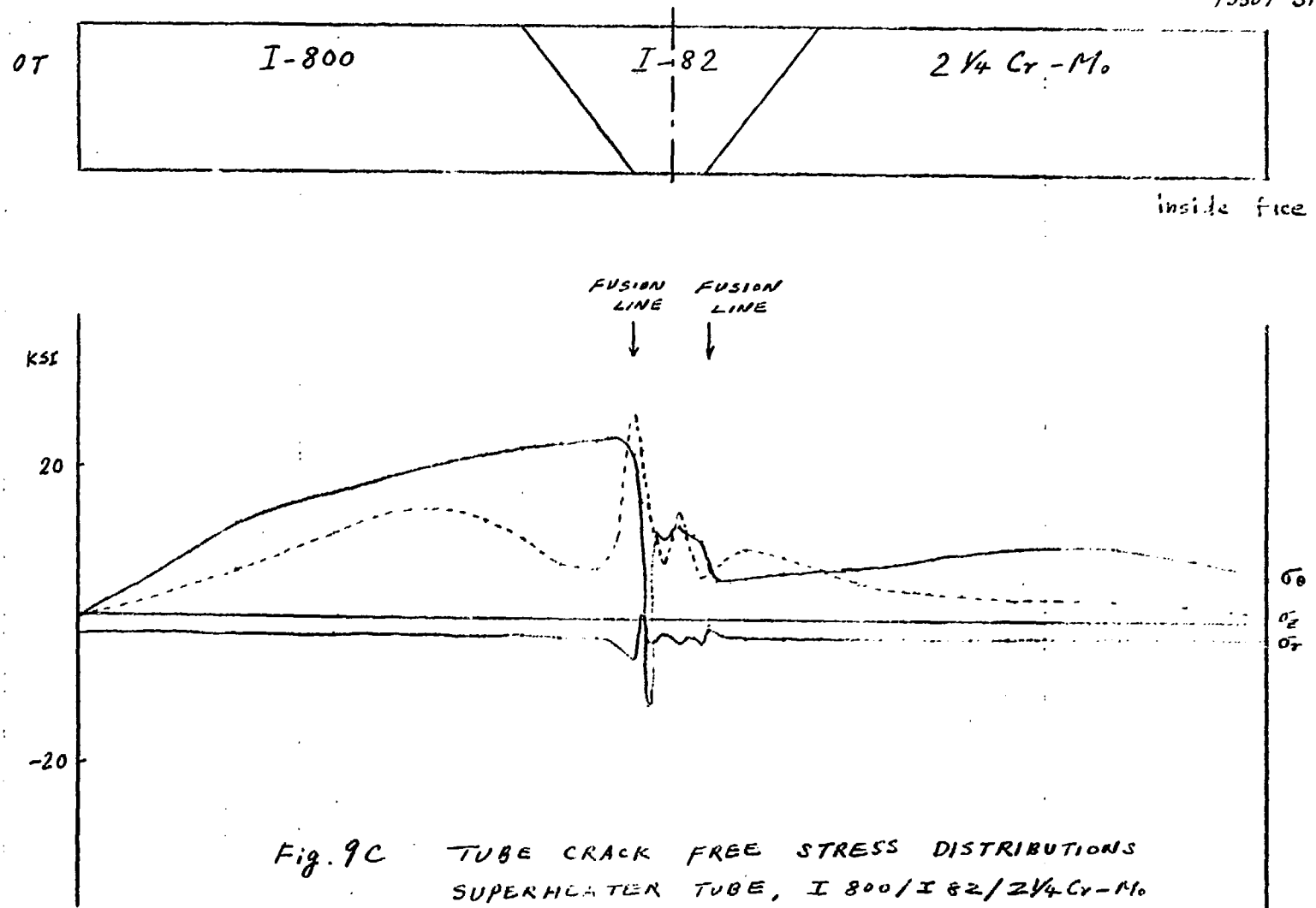

Fig. 9C TUBE CRACK FREE STRESS DISTRIBUTIONS
SUPERHEATER TUBE, I 800/I 82/2¼ Cr-Mo
STRESS FREE AT 1350°F

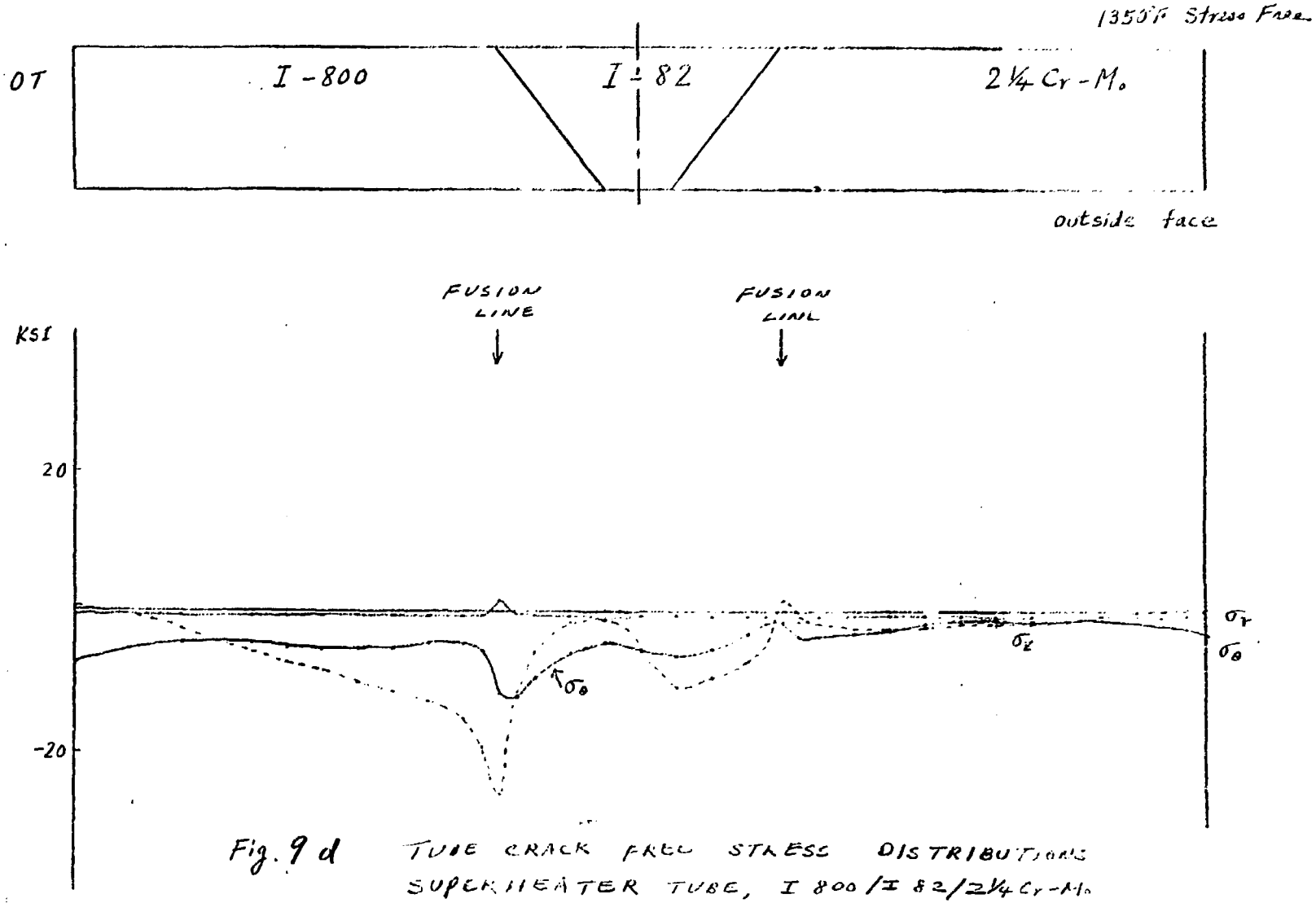

Fig. 9 d TUBE CRACK FREE STRESS DISTRIBUTIONS SUPERHEATER TUBE, I 800/I 82/2¼ Cr-Mo STRESS FREE AT 1350°F

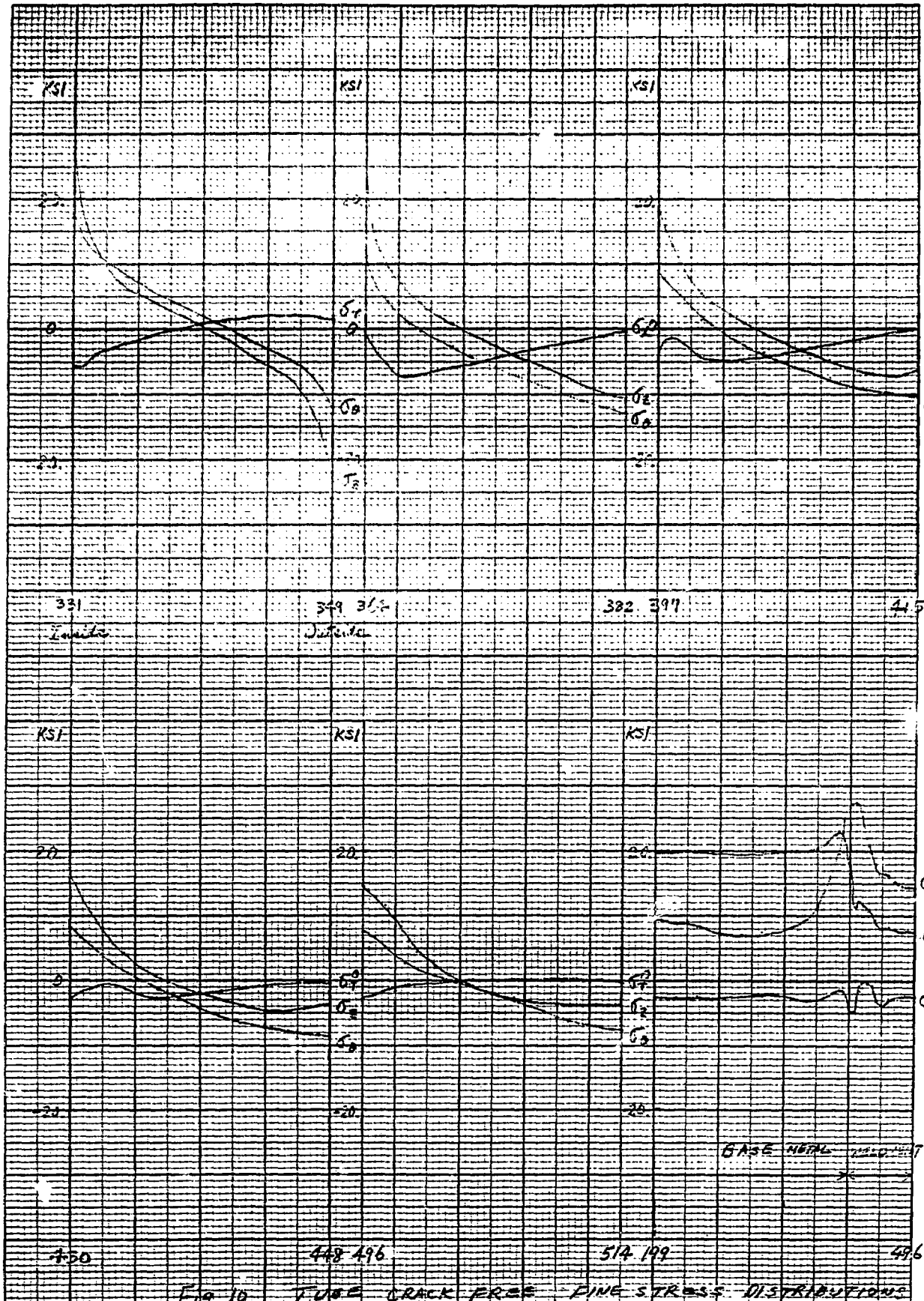

Fig. 10 TUBE CRACK FREE PINE STRESS DISTRIBUTIONS
SUPERHEATER TUBE, I850/I82/I850
STRESS FREE AT 1350°F

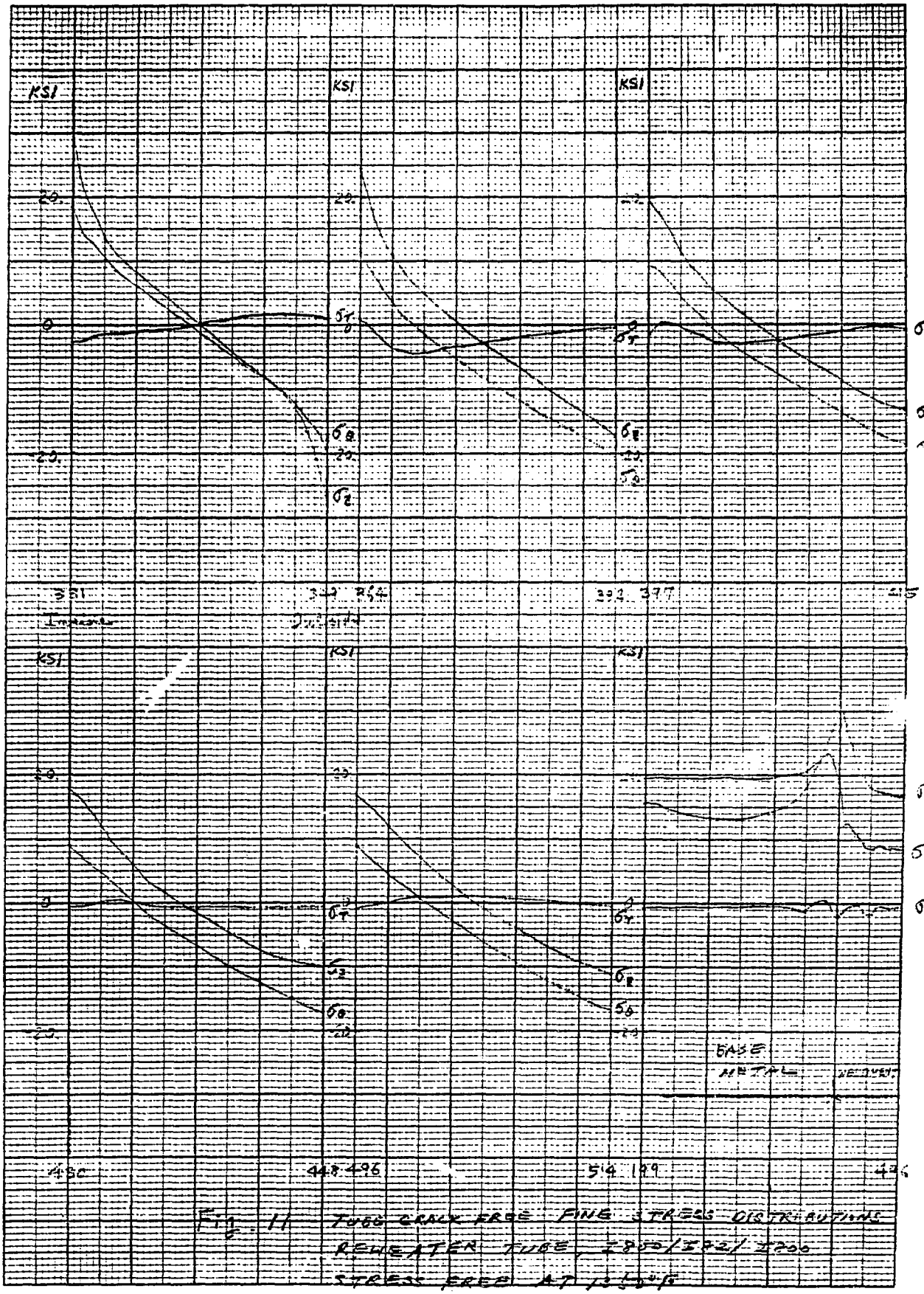

Fig. 11 TUBE CRACK FREE FINE STRESS DISTRIBUTIONS REHEATER TUBE T250/T22/T200 STRESS FREE AT 1150°F

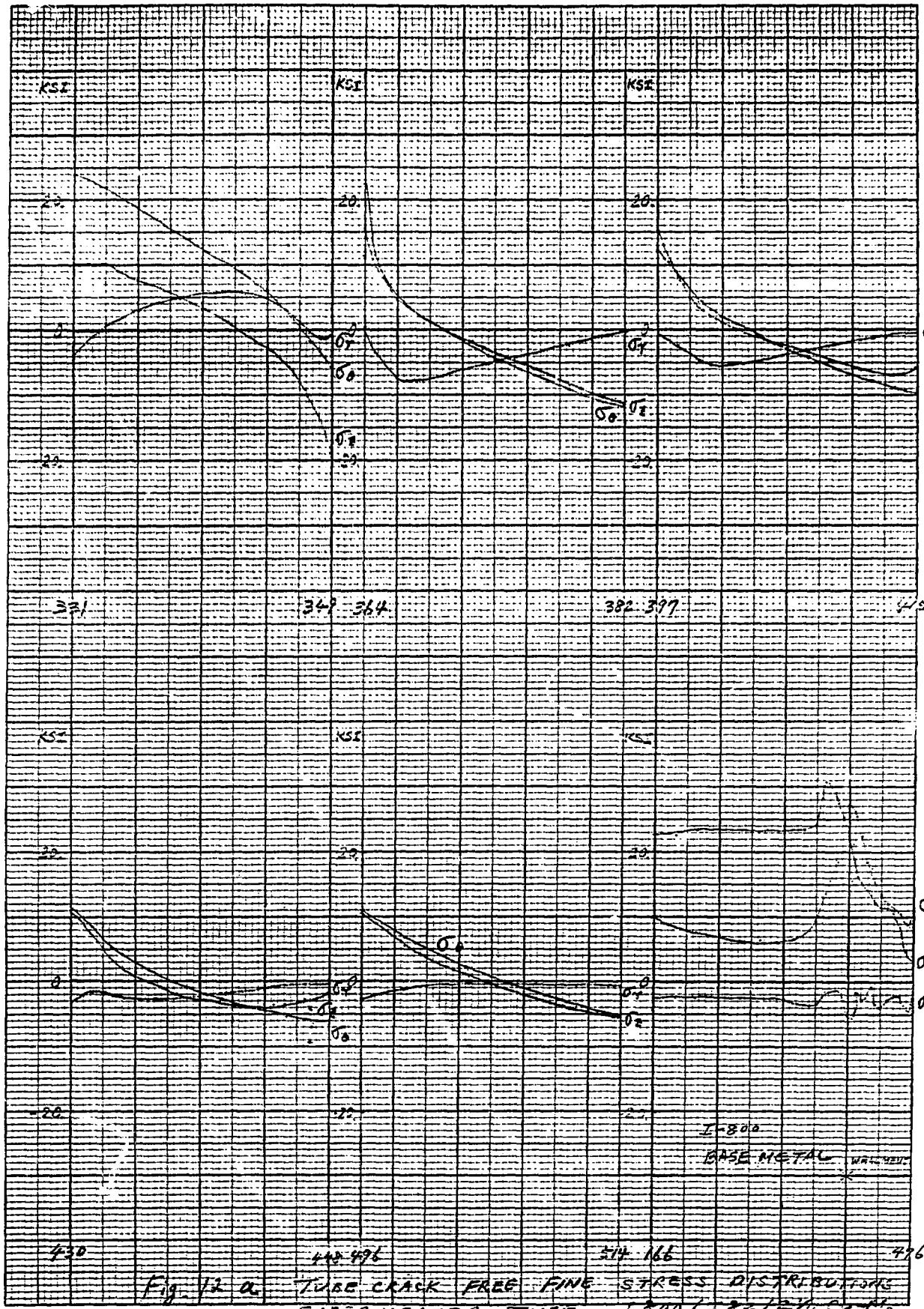

Fig. 12a TUBE CRACK FREE FINE STRESS DISTRIBUTIONS SUPERHEATER TUBE, 1800/182/2½ CP AS STRESS FREE AT 1350°F

GRAPH PAPER GRAPHIC CONTROLS CORPORATION Buffalo New York Printed in U.S.A.
SQUARE 10 X 10 TO THE INCH

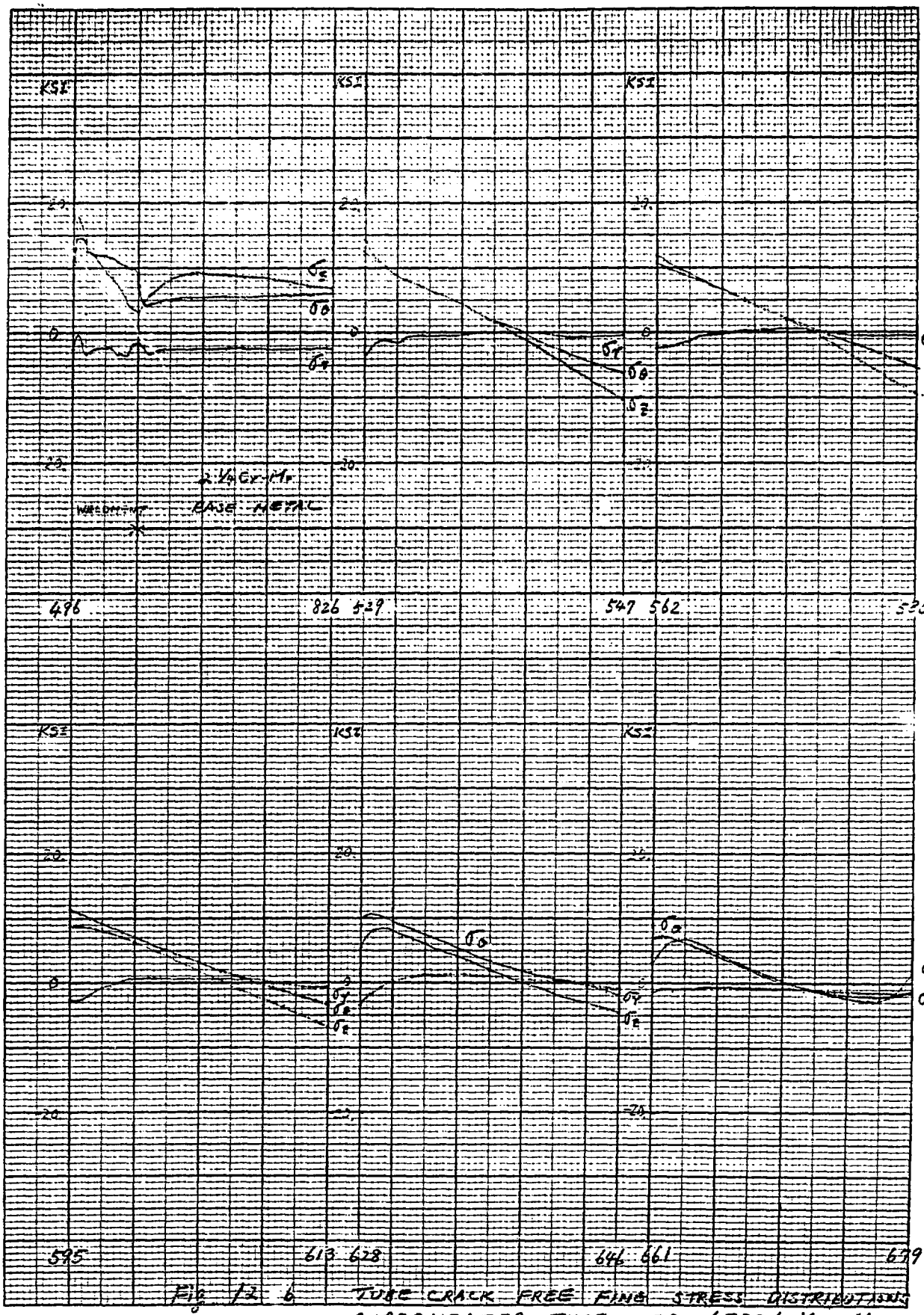

Fig 12 6 TUBE CRACK FREE FINS STRESS DISTRIBUTIONS
SUPERHEATER TUBE, I800/I82/2¼Cr-1Mo
STRESS FREE AT 1350°F

GRAPH PAPER GRAPHIC CONTROLS CORPORATION Buffalo, New York Printed in U.S.A. SQUARE 10 X 10 TO THE HALF INCH AS 0013 01

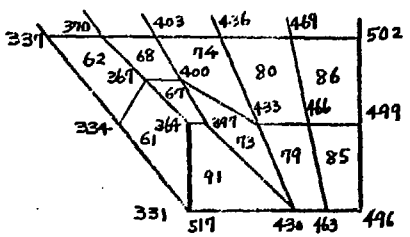

(a) $a/t = 0.0125$

where a = crack length

t = wall thickness

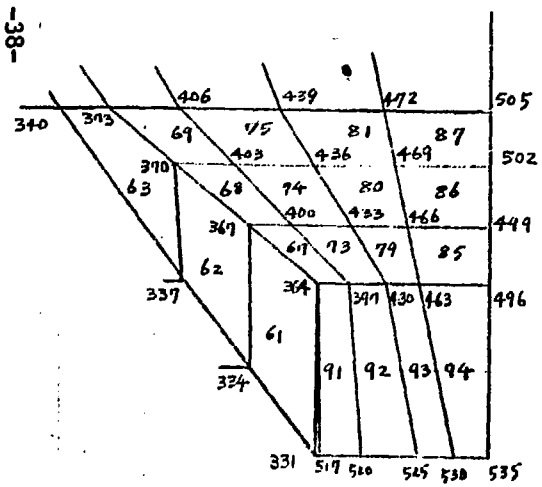

(b) $a/t = 0.025$

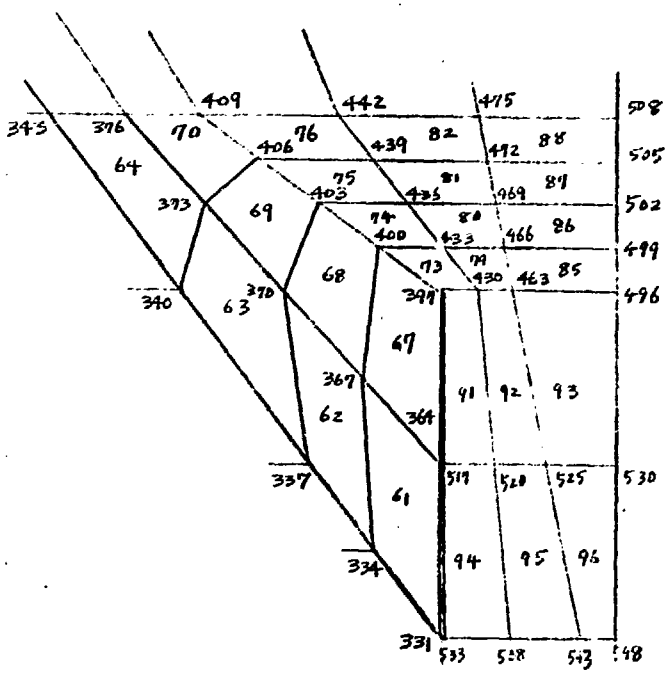

(c) $a/t = 0.5$

Figure 13. Idealizations for Fracture Mechanics Calculations

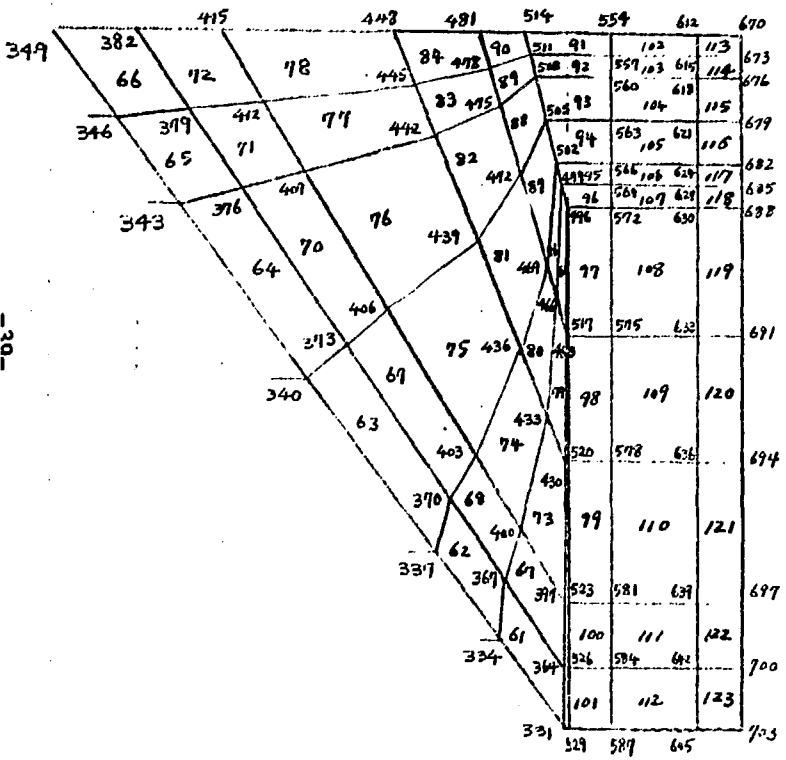

(d) $a/t = 0.75$

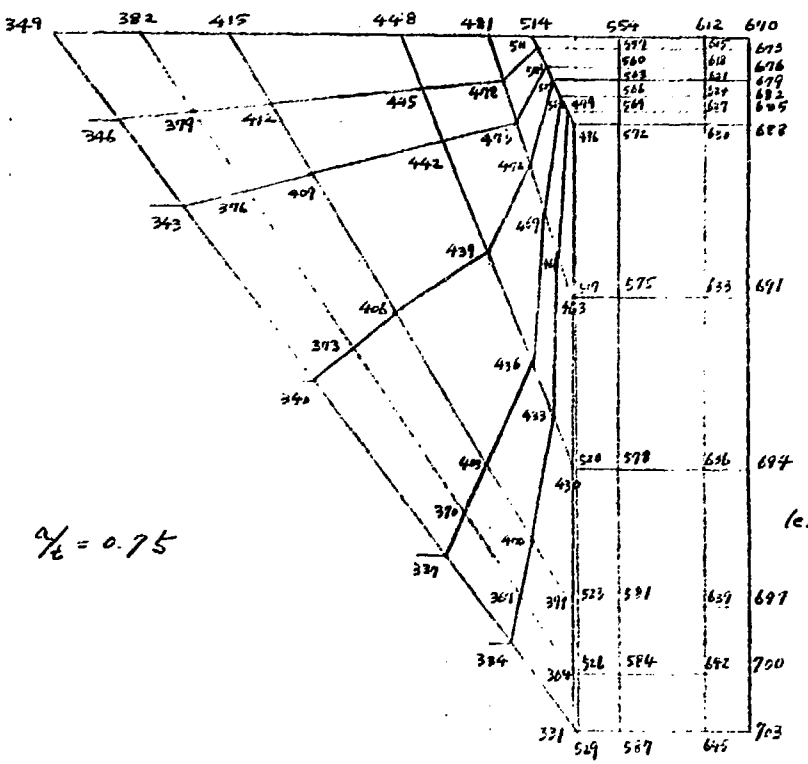

(e) $a/t = 0.875$

Figure 13. Idealizations for Fracture Mechanics Calculations

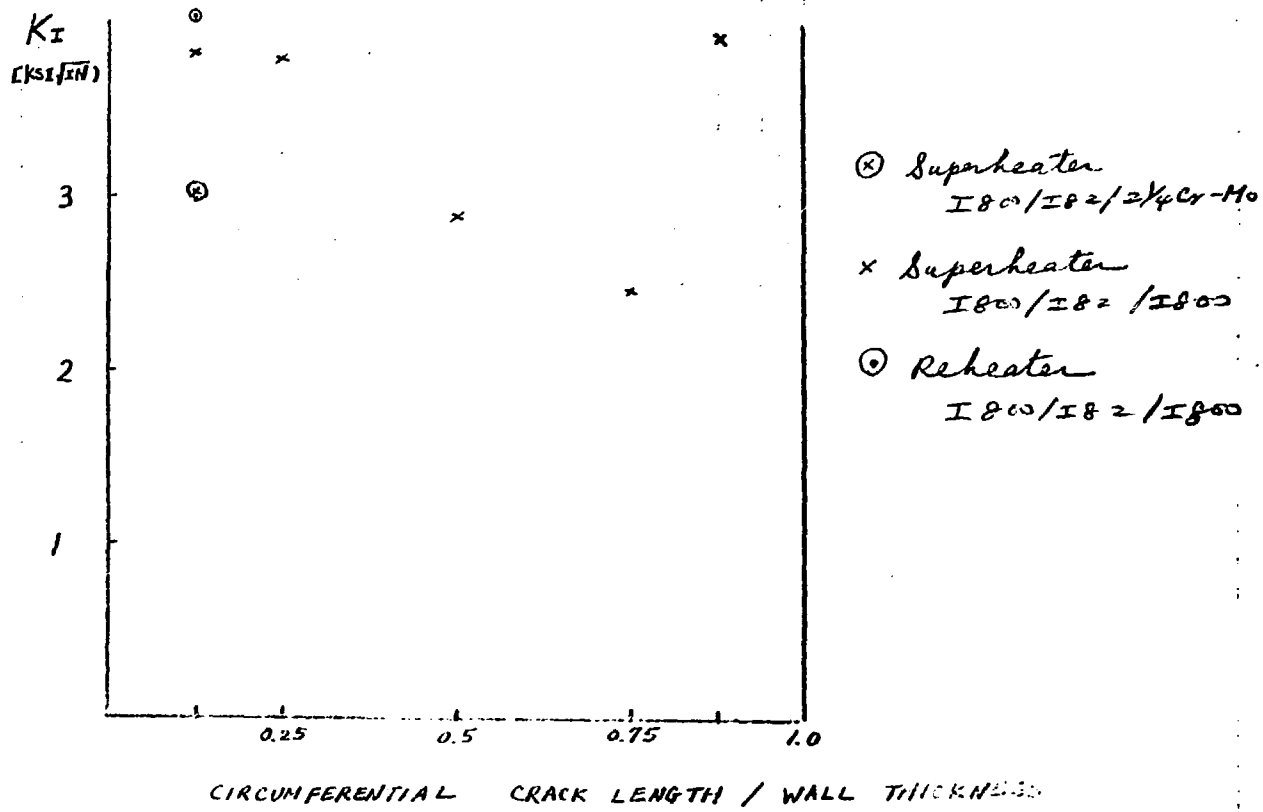

Fig. 14 Computed Stress Intensity Factors at Operating Temperature, Stress Free at 1350°F

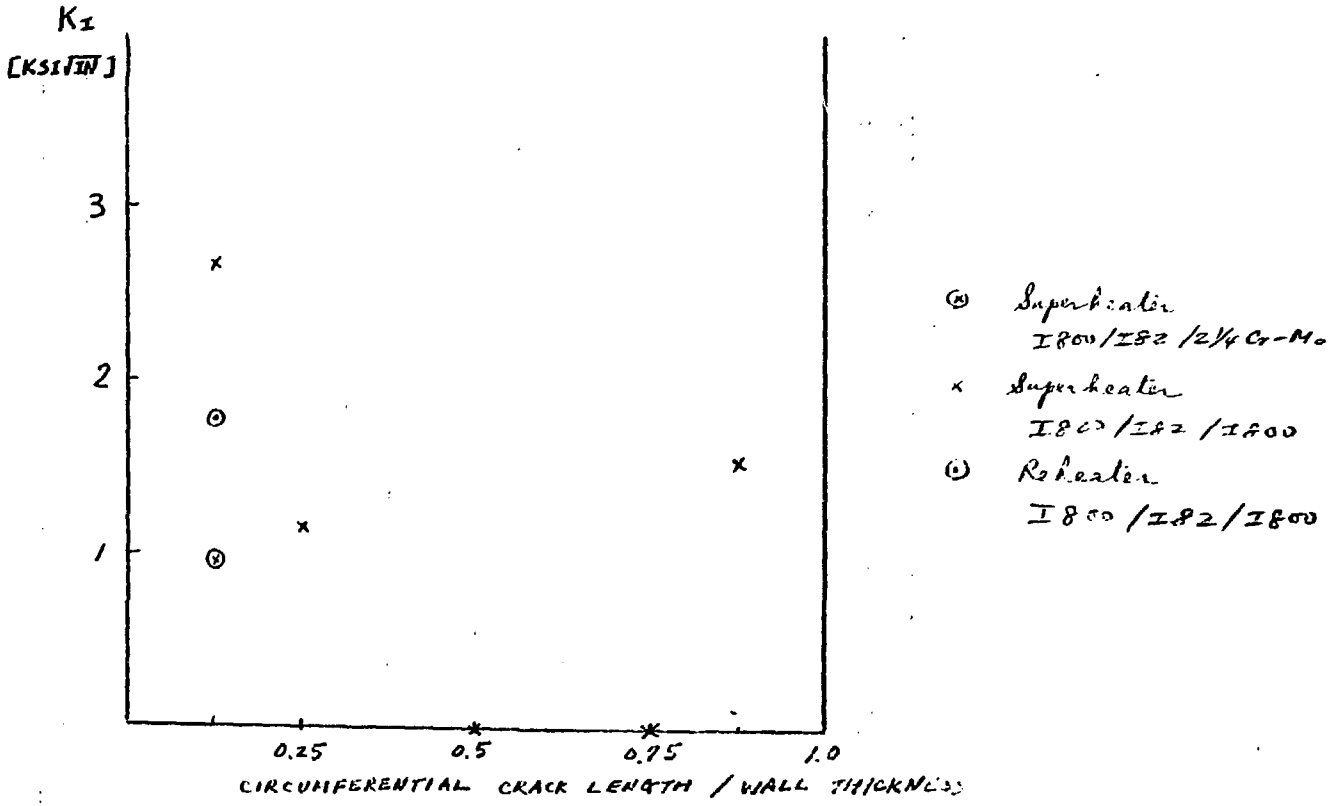

Fig. 15 Computed Stress Intensity Factors at Room Temperature, Stress Free at 1350°F

APPENDIX

Validation of Apes Fracture Mechanics Calculation

The APES computer code was modified to increase the number of nodes (400 → 1500), elements (50 → 200) and nodes across the front (40 → 80), and to include the capability of analyzing thermal loading conditions. The code was checked out with the supplied, as well as newly developed test problems. The validation of the APES fracture mechanics calculations is described below.

1. Single-Edge Crack in a Compact Tension Specimen

The problem of a plate 5 units square and containing a central edge crack of length a=1.5 units was considered. The problem is symmetric about the crack line and treated as a plane-strain problem. The reference value for K for this specimen geometry is 4.016. The APES results for K (4.096 and 4.080) shown in Figure A-1 and A-2 were 2.0 percent higher than the reference value.

2. 45-Degree Slant Crack in a Tension Specimen

This example is a combined node plane strain problem. The geometry is shown in Figure A-3 and A-4 along with the finite element idealizations used. The computed results for K_I and K_{II} are also shown in the Figures. The reference values of K_I and K_{II} are 1.86 and 0.88. The results shown in Figure A-3 indicate that the value of K_I varied from 4.0 percent below to 2.4 percent above the reference value and that the value of K_{II} varied from 2.9 percent below to 1.4 percent above the reference value. For an isothermal loading case the values of K_I and K_{II} are zero as expected.

The results using a core crack tip element are shown in Figure A-4. They indicate that the value of K_I was 24 percent below the reference value and K_{II} was 30 percent below the reference value.

3. Cracked Bar

This problem was a bar with a circumferential crack with a depth of half the bar radius. The results shown in Figure A-5 indicate that the value of K was 7.6% below the reference value.

4. Cylinder with Internal Circumferential or Internal Axial Cracks

For the analysis cylinders with internal circumferential or internal axial cracks were evaluated. Loading conditions similar to those used for the Incoloy-800 superheater tube were used. The results shown in Figure A-6 and A-7 were compared with those developed below using the weight function concept.

The crack opening stress $\sigma(x)$ can be approximated by a polynomial.

$$\sigma(x) = \sigma_o + \{\frac{x}{B}\}\sigma_1 + \{\frac{x}{B}\}^2\sigma_2 + \text{----------} + \{\frac{x}{B}\}^m\sigma_m \qquad (1)$$

For a crack subjected to a node I pressure $\sigma(x)$, the stress intensity factor can be calculated when the weight function $m(\frac{x}{a}, \frac{a}{B})$ is known for the crack geometry.

$$K = \sqrt{\frac{2}{\pi}}\int_o^a \frac{m(\frac{x}{a}, \frac{a}{B})}{\sqrt{a-x}}\,\sigma(x)dx \qquad (2)$$

Substituting Eq. (1) into Eq. (2) yields

$$K = \sqrt{\pi a}\left[\sigma_o i_o(\frac{a}{B}) + \{\frac{a}{B}\}\sigma_1 i_1(\frac{a}{B}) + \text{---------} + \{\frac{a}{B}\}^m\sigma_m i_m\{\frac{a}{B}\}\right] \qquad (3)$$

and

$$i_j(\frac{a}{B}) = \frac{1}{\pi}\sqrt{\frac{2}{a}}\int_o^a \{\frac{x}{a}\}^j \frac{m(\frac{a}{a}, \frac{a}{B})}{\sqrt{a-x}}\,dx \qquad (4)$$

The value of i_j can be calculated exactly or by using an appropriate numerical method. The limit values of $i_j\ (\frac{a}{B})$ when $a/B \to o$ are the same for all cracks in all structures, that of a crack in a semi-infinite half plane.

These limit values can be calculated using Eq. (4) and the following Equation (5).

$$m\ \{\frac{x}{a},o\} = 1 + 0.6147\ \{1 - \frac{x}{a}\} + 0.2502\ \{1 - \frac{x}{a}\}^2 \qquad (5)$$

Limit values of i_j when $a/B \to o$ were taken from J. Heliot and J. Vagner.*

j	0	1	2	3	4
$i_j(0)$	1.12	0.687	0.528	0.446	0.389

For the present analysis ($a/B = 0.125$ and $R/B = 1.825$) $i_j\ (a/B)$ can be approximated to be $i_j(0)$. Thus Eq. (3) can be given by

$$K = \sqrt{\pi a}\left\{1.12\ \sigma_o + 0.687\ \{\frac{a}{B}\}\ \sigma_1 + 0.528\ \{\frac{a}{B}\}^2\sigma_2 + 0.446\ \{\frac{a}{B}\}^3\sigma_3 + 0.389\ \{\frac{a}{B}\}^4\sigma_4\right\} \qquad (6)$$

The stress distribution predicted with the present model is shown in Figure A-8 for an approximate stress function.

The stress intensity factor can then be calculated using Eq. (6). The results are shown below as well as the values predicted with APES.

* Heliot, J. and Vagner, J., "Use of the weight function concept and the crack closing method for calculating stress intensity factors in plane or axisymmetric problems," MS 241, ICF 4, Waterloo, 1977.

		Reference Value	APES Value
Circumferential Crack	Plane Strain	10[illegible],000	109468.5
	Axisymmetric	32,266	32544.8
Axial Crack	Plane Strain	3,355	3589.7

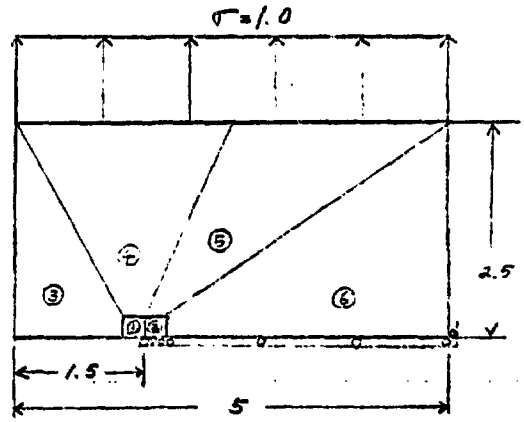

$K_{Ref} = 4.016$*

$K = 4.09653$

Figure A-1. Idealization of Single-Edge Crack by Enriched QUAD-12 Elements

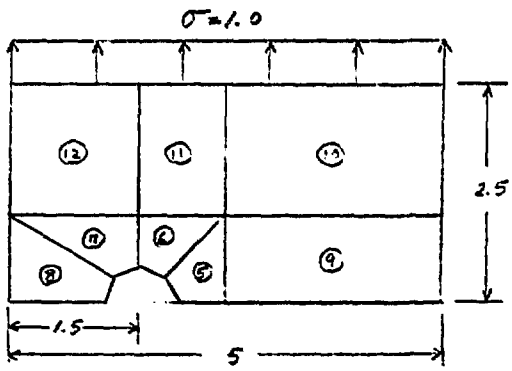

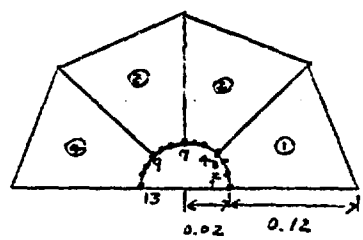

$K_{Ref} = 4.016$

$K = 4.0793$

Figure A-2. Idealization of Single-Edge Crack by Core Element with 13 nodes

* Bowie, O.L. and Neal, D.M., "Single Edge Crack in a Rectangular Tensile Sheet," J. Appl. Mech., Vol. 32 (1965)

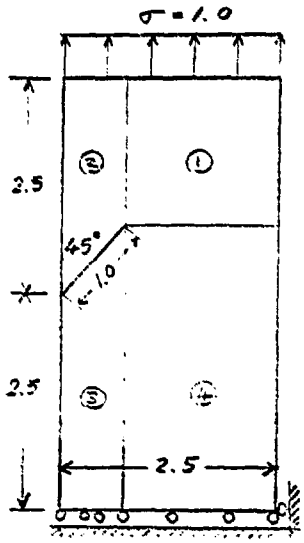

4 Elements

$K_1 = 1.78636$

$K_2 = 0.85406$

Ref*: $K_1 = 1.86$

$K_2 = 0.83$

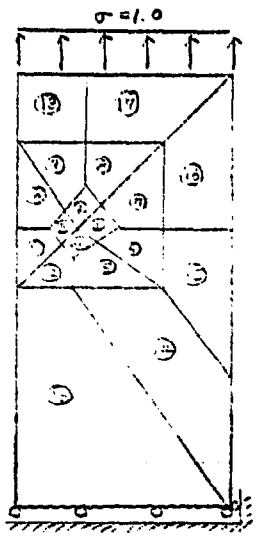

18 Elements

$K_1 = 1.20583$

$K_2 = 0.89196$

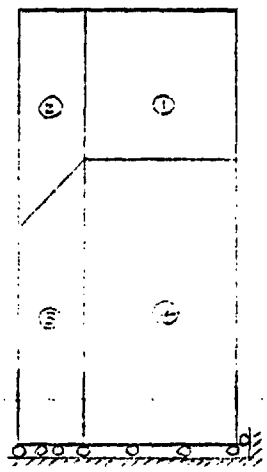

4 Elements

$K_1 = 0.00001$

$K_2 = -0.00001$

Figure A-3 Idealization of 45-Degree Slant Crack in Tension Specimen

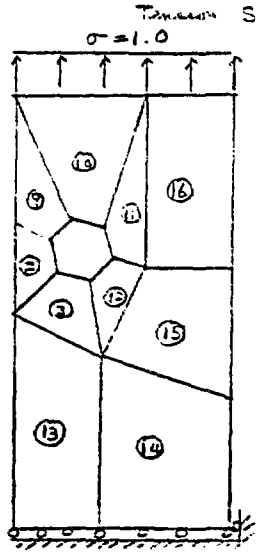

$K_1 = 1.4161$

$K_2 = 0.6182$

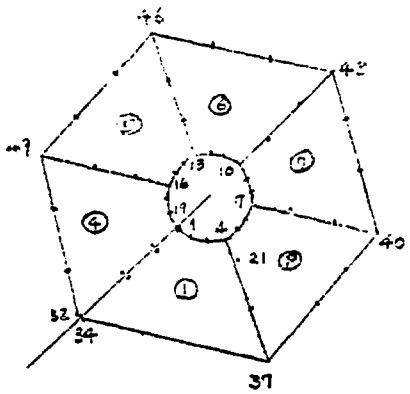

Figure A-4 Idealization of Single-Edge Crack by Core Element with 19 Nodes

* Bowie, O.L., "Solution of Plane Crack Problems by Mapping Techniques," "Mechanics of Fracture," Vol. 1, pp. 1-55, Noordhoff, Leyden, Netherlands (1973).

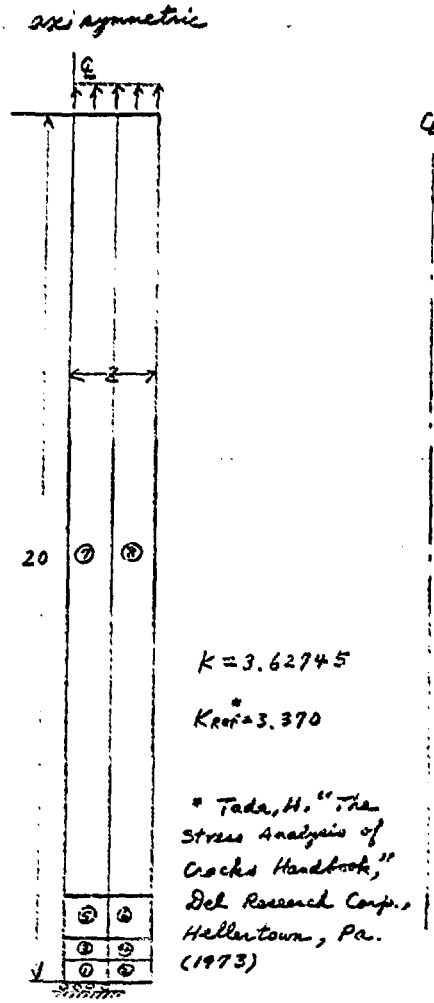

Figure A-5 Idealization of Cracked Bar

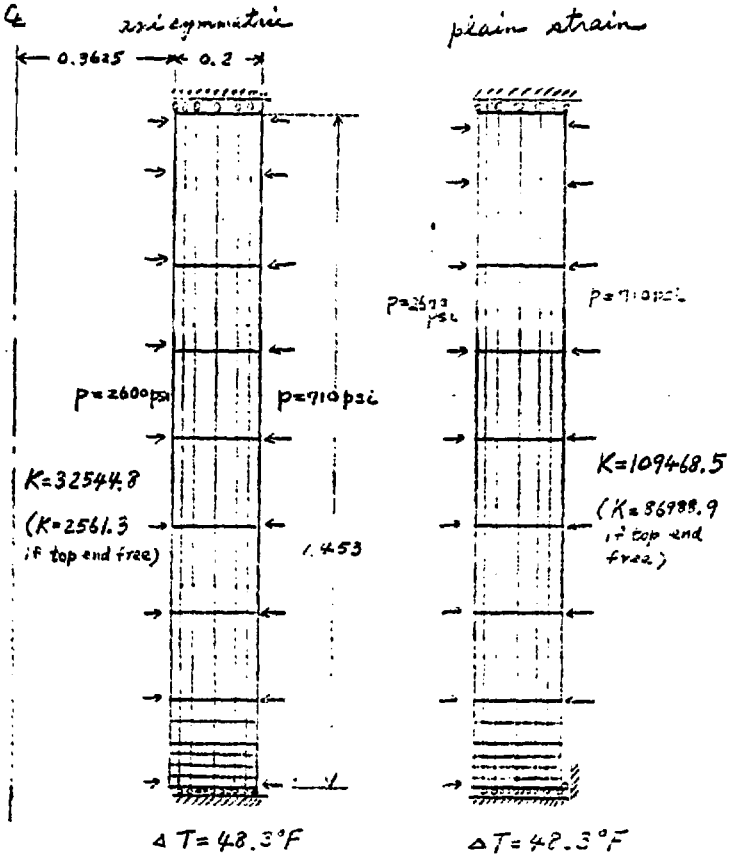

Figure A-6 Idealization of Cylinder with Internal Circumferential Crack

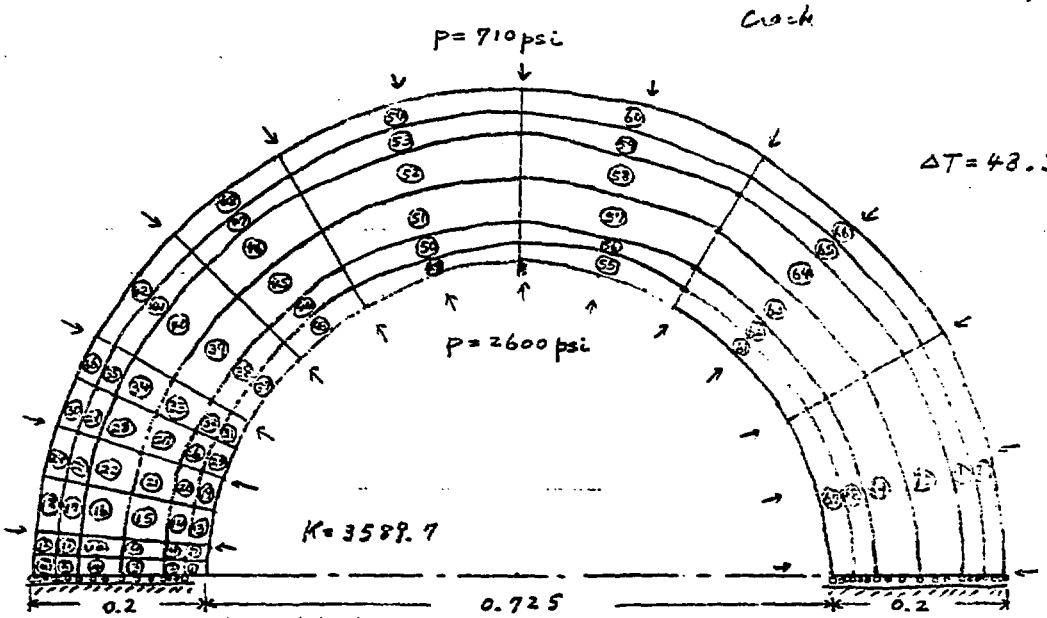

Figure A-7 Idealization of Cylinder with Internal Axial Crack

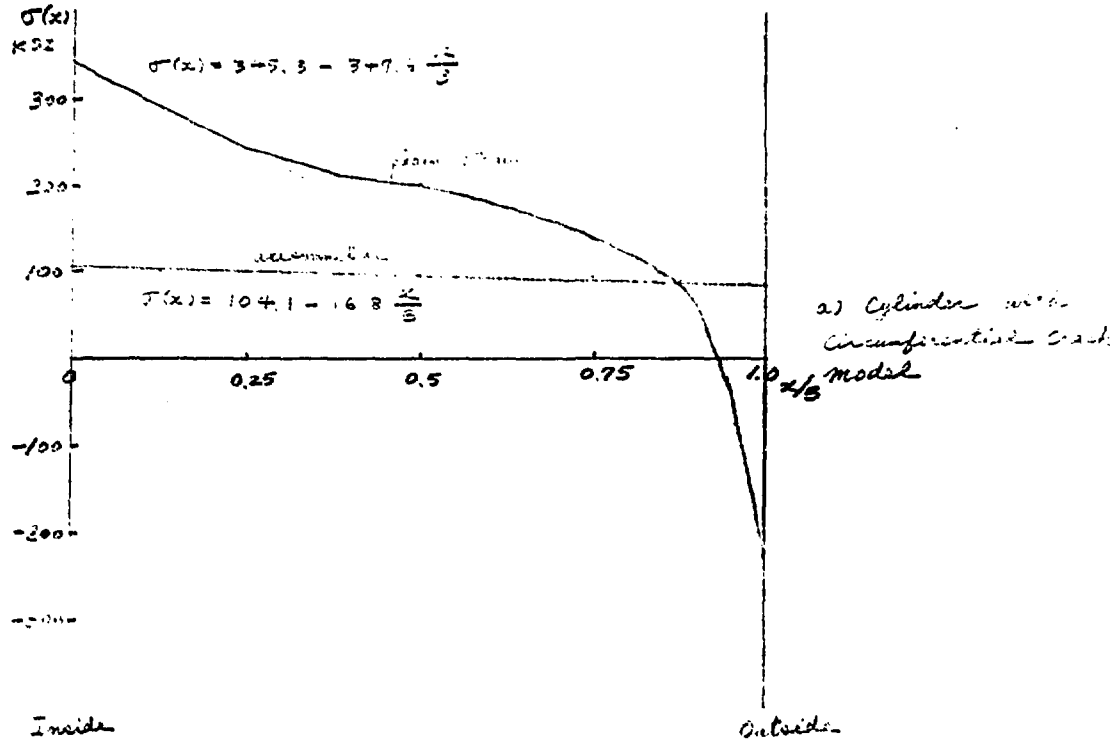

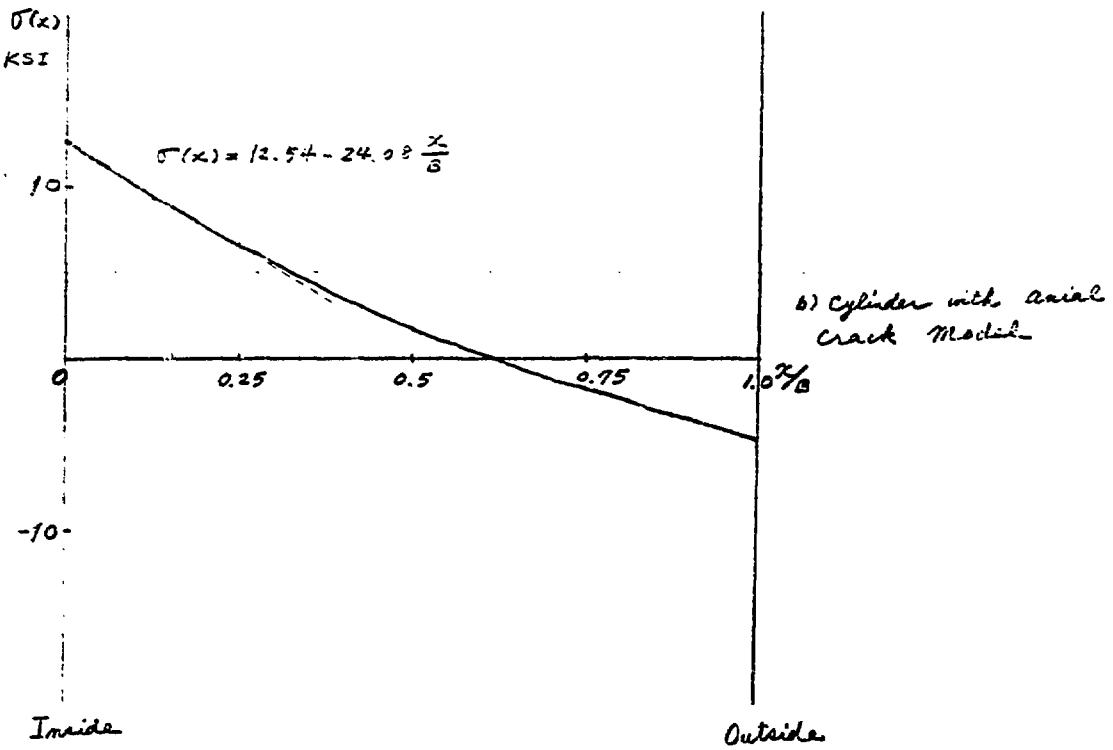

Figure A-8 Crack Opening Stress σ(x) Distribution